HIGHWAY RESEARCH RECORD

Number 438 | Soil Compaction and Corrugations

6 reports
prepared for the
52nd Annual Meeting

Subject Areas

33	Construction
34	General Materials
61	Exploration-Classification (Soils)
62	Foundations (Soils)
64	Soil Science

HIGHWAY RESEARCH BOARD

DIVISION OF ENGINEERING NATIONAL RESEARCH COUNCIL
NATIONAL ACADEMY OF SCIENCES—NATIONAL ACADEMY OF ENGINEERING

Washington, D.C. 1973

NOTICE

The studies reported herein were not undertaken under the aegis of the National Academy of Sciences or the National Research Council. The papers report research work of the authors that was done at the institutions named by the authors. The papers were offered to the Highway Research Board of the National Research Council for publication and are published here in the interest of the dissemination of information from research, one of the major functions of the Highway Research Board.

Before publication, each paper was reviewed by members of the HRB committee named as its sponsor and accepted as objective, useful, and suitable for publication by the National Research Council. The members of the review committee were chosen for recognized scholarly competence and with due consideration for the balance of disciplines appropriate to the subject concerned.

Responsibility for the publication of these reports rests with the sponsoring committee. However, the opinions and conclusions expressed in the reports are those of the individual authors and not necessarily those of the sponsoring committee, the Highway Research Board, or the National Research Council.

Each report is reviewed and processed according to the procedures established and monitored by the Report Review Committee of the National Academy of Sciences. Distribution of the report is approved by the President of the Academy upon satisfactory completion of the review process.

ISBN 0-309-02169-3
Library of Congress Catalog Card No. 73-10631
Price: $2.20

Highway Research Board publications are available by ordering directly from the Board. They are also obtainable on a regular basis through organizational or individual supporting membership in the Board; members or library subscribers are eligible for substantial discounts. For further information write to the Highway Research Board, National Academy of Sciences, 2101 Constitution Avenue N.W., Washington, D.C. 20418.

CONTENTS

FOREWORD

Uniform subgrade support that will provide a more satisfactory riding surface is the objective of continuing research on soil compaction. Improvements in earthwork construction will be enhanced by the additional knowledge presented in this RECORD concerning compaction fundamentals, control curves, specifications, and evaluations.

Majidzadeh and Guirguis report on the correlation between engineering and physical properties of field- and laboratory-compacted specimens. In their studies, they are trying to improve the prediction of pavement performance under severe service conditions. Lee and Hsu studied oddly shaped compaction curves to try to assess the effects of temperature on them. Irregular curves are often confusing to those entrusted with field compaction control, and this study is an attempt to clear up some of that confusion. Kraft and Yeung developed the failure probability of linear elastic, heterogeneous embankments and suggest how the results can be incorporated into acceptance specifications. Selig applies strain measurements to the evaluation of soil compactors. The measurements were found to be useful in evaluating the variations with depth, changes with compactive effort, effects of succeeding layers, compactor capability, and assessment of variability. Smith discusses the various factors that affect the calibration of nuclear moisture gauges.

Riley and Furry present a study of road corrugations and conclude that there are maximum as well as minimum values of vehicle weight, tire pressure, and vehicle speed above or below which corrugation will not occur.

FUNDAMENTALS OF SOIL COMPACTION AND PERFORMANCE

Kamran Majidzadeh and Hani R. Guirguis, Ohio State University

The overall objectives of this research study were to develop methods of predicting pavement performance under severe service conditions; to arrive at a more rapid, accurate means of controlling the quality of the compaction process; to predict, from a limited laboratory study, the quality of subgrade soil required for the anticipated service conditions; and to ensure that the desired material properties are attained during construction. The research was carried out primarily to study the correlation between engineering and physical properties of field- and laboratory-compacted specimens. Undisturbed field specimens were obtained after regular sheepsfoot-roller compaction, regular proof rolling, and extra proof rolling. The parameters evaluated were physical characteristic, primary response, and ultimate response. The combined effects of compactive effort, type of compaction, moisture content at compaction, and moisture gain after compaction on the physical parameters and engineering properties were noted and compared for field- and laboratory-prepared soil. This study shows that the physical soil parameters describing the interrelation among moisture, density, compaction energy, and method of compaction can be used for the correlation of laboratory and field specimens. Comparing shear strength characteristics of laboratory and field specimens at various moisture contents and compaction conditions indicated that the laboratory gyratory method and the 40-blow drop-hammer method are more representative of the field-compaction process. The creep modulus, dynamic modulus, and resilient modulus can be used to interrelate properties of field- and laboratory-compacted specimens. The relations presented in this report indicate that maximum moduli occur at approximately the same moisture content as the optimum dry density and shear strength.

•THE ABILITY of any rational design method to predict the stress-strain-environment-time response of the pavement system depends on the knowledge of material properties that best measure performance. The subgrade soil is considered to be an important component of the pavement system, and its contribution to the performance level depends on its in situ characteristics. In many engineering analyses, the physical characteristics of soils such as moisture and density are used and in turn are translated into the efficiency of the compaction process. The mechanics of the compaction process, field and laboratory methods of soil densification, and methods of evaluation of properties of compacted soil have been discussed in great length in the published literature (1, 2, 3, 4).

It has been recognized (5, 6, 7, 8) that the soil compaction process affects a variety of properties that can be broadly categorized into 2 interrelated types: physical and engineering properties. The physical properties, i.e., the moisture and density, can be used to analyze the efficiency of the compaction process. However, engineers are interested not only in density per se but also in its effect on the engineering properties describing the soil-support conditions.

It has been demonstrated that soils compacted to a given density and moisture content may exhibit different engineering properties depending on the method of compaction used and the soil structure developed by the application of compaction energy. Because physical properties cannot fully satisfy all requirements of pavement design and performance evaluation, there is a question of what limiting engineering properties need to be selected.

In the search for suitable engineering properties to be used in the evaluation of laboratory- and field-compacted specimens, many researchers have investigated rheological and strength-deformation characteristics of subgrade soils as affected by the compaction process and environmental conditions (9, 10, 11, 12, 13, 14). The nature of the material response to changes in climatic and loading conditions has been extensively used as a basis for the characterization of soils within the framework of elastic, viscous, viscoelastic, and elastic-plastic theories. The analysis of soil behavior presented in this study can be placed into 2 categories: (a) properties describing the non-failure-state response (primary response) and (b) properties describing the failure-state reponse (ultimate response). The non-failure-state response can be characterized by creep, relaxation, dynamic modulus, and resilient modulus. The failure-state response includes both unconfined compressive or shear strength and failure under repeated loading.

The rate process theory and accumulated plastic deformation concepts are used to explain the process of deformation and failure under repeated loading. In this study, special attention is given to the following parameters, which are suggested to be a measure of subgrade performance: (a) resilience modulus and response under repeated loading; (b) shear strength; and (c) rutting deformation, resultant densification, and cumulative damage under repeated loading. Other parameters, such as soil suction-moisture relation and frost susceptibility, are also considered as important performance parameters, but they are not discussed in this paper.

TESTING PROCEDURES AND MATERIAL CHARACTERISTICS

The material used in this investigation is a silty clay soil obtained from Allen County, Ohio (US-30, Project 433-1969). Two types of specimens were used: undisturbed field cores and laboratory-compacted specimens. The undisturbed samples were taken from the subgrade embankment by means of a 3-in. internal diameter Shelby tube; the dry boring method was used. The specimens were taken after varying amounts of compaction effort had been applied to the soil. The compaction levels at which undisturbed soil samples were obtained are as follows: (a) regular sheepsfoot rolling, (b) proof rolling at regular speed, (c) 3 passes of proof rolling at regular speed, and (d) 3 passes of proof rolling at regular speed and 1 pass at double speed.

In this study, laboratory specimens were prepared by drop-hammer and gyratory compaction. For the drop-hammer compaction, the compaction energy varied by the total number of blows imparted to the specimen. The number of blows ranged from 25 to 70; 40 blows correspond to the modified AASHO compaction energy input. For gyratory compaction, the angle of gyration and the number of gyrations were kept at 2 deg and 15 gyrations. The axial static pressure was 700 and 100 lb. The physical characteristics of the soil used in this study are as follows:

Characteristic	Value
Liquid limit	37
Plastic limit	19
Specific gravity	2.78
Unified classification	CL
AASHO classification	A-6

The moisture-density relation of drop-hammer- and gyratory-compacted specimens is shown in Figures 1 and 2. In Figure 1, the moisture-density relation of undisturbed soil samples is superimposed on the moisture-density data for drop-hammer compaction. It appears that field data are primarily on the wet side of optimum.

Figure 1. Field moisture content versus density with drop-hammer compaction.

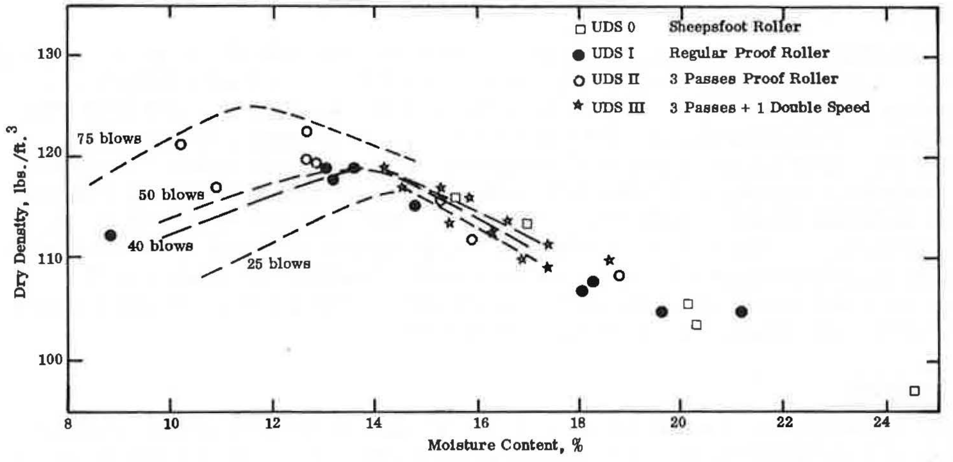

Figure 2. Dry density and unconfined compressive strength versus moisture content with gyratory compaction.

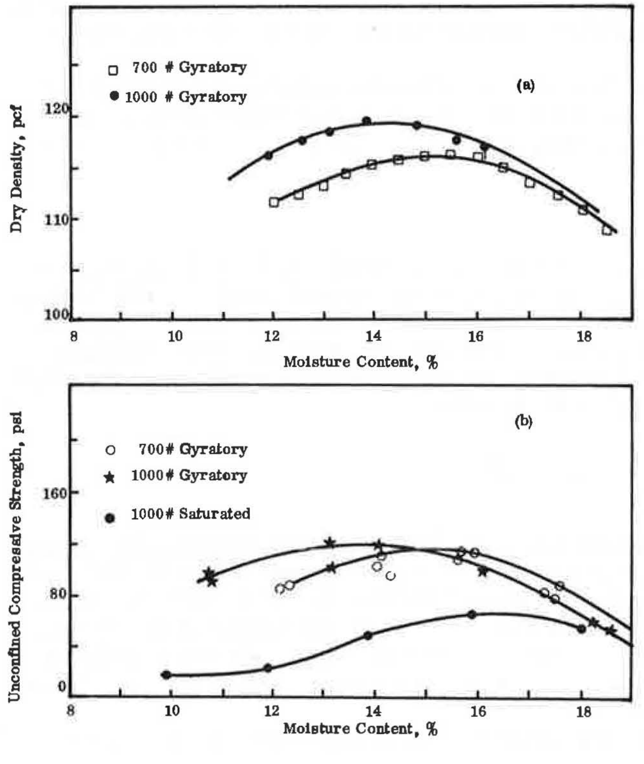

PRIMARY RESPONSE

Creep Function

The deformation-time response of a material body under constant stress, i.e., creep, is extensively used for characterizing engineering systems. The creep compliance J(t), defined as strain per unit stress, or its inverse creep modulus E_c, has been used in the characterization of subgrade soils as well as other pavement materials.

So that deformation characteristics of compacted soils can be compared at various moisture contents, compactive efforts, and methods of compaction, the creep modulus E_c has been determined at t = 1,500 sec. The E_c-moisture content relation exhibits a similar trend to moisture-density and shear strength-moisture content relations (Fig. 3). The optimum moisture content for E_c-moisture content relation for drop-hammer- and gyratory-compacted specimens agrees closely with the corresponding optimum moisture content for moisture-density-shear strength relations.

Dynamic Modulus

The dynamic response of material systems is characterized by dynamic modulus $/E^*/$, which is considered to be one of the major primary response mode parameters. The dynamic modulus can be determined either directly from the dynamic experiments or from the transformation of creep compliance data into the frequency domain.

Figure 4 shows the dynamic moduli of compacted laboratory and field specimens at various moisture contents with various compaction levels. The curves are similar to those shown for the creep modulus-moisture content relations. Similarly, the optimum moisture content agrees well with the optimum moisture content for density, shear strength, and creep modulus.

The comparison of data indicates that, at high moisture contents (greater than 16 percent), the agreement is rather poor but that, within the range of optimum moisture content, the field data agree well with either 700 lb of gyratory or 40 blows of drop-hammer compaction.

Resilient Modulus

The sinusoidal loading functions used for the determination of dynamic modulus were an oversimplification of actual loading patterns occurring in pavements. Traffic loading patterns were simulated in the laboratory by experiments that used pulsating dynamic loads of varying frequency and rest periods. The modulus characterizing material response under such dynamic loading is known as the modulus of resilience, M_R, which was calculated for each load cycle from the relation

$$M_R = \frac{\sigma}{\epsilon_d}$$

where σ is the repeatedly applied stress and ϵ_d is the resilient or recoverable strain. In general, 2 types of relations were observed: At stresses greater than the endurance limit, M_R decreased with increasing N; at stresses smaller than the endurance limit, M_R increased with increasing N. The first type of behavior was possibly because of work softening, while the latter was a result of work hardening. Above the endurance limit, the structural changes induced are nonreversible and are caused by cumulative damage within the material system.

In general, the relation of M_R with the number of load repetitions N can be expressed as an approximation by

$$M_R = A\, N^{\alpha(\sigma)}$$

where α depends on the stress level or more precisely on the ratio of applied stress to strength. For stresses below the endurance limit, α is more than unity; for stresses large enough to result in damage, i.e., greater than endurance limit, α is less than unity.

Figure 3. Dynamic moduli versus moisture content with various compaction methods.

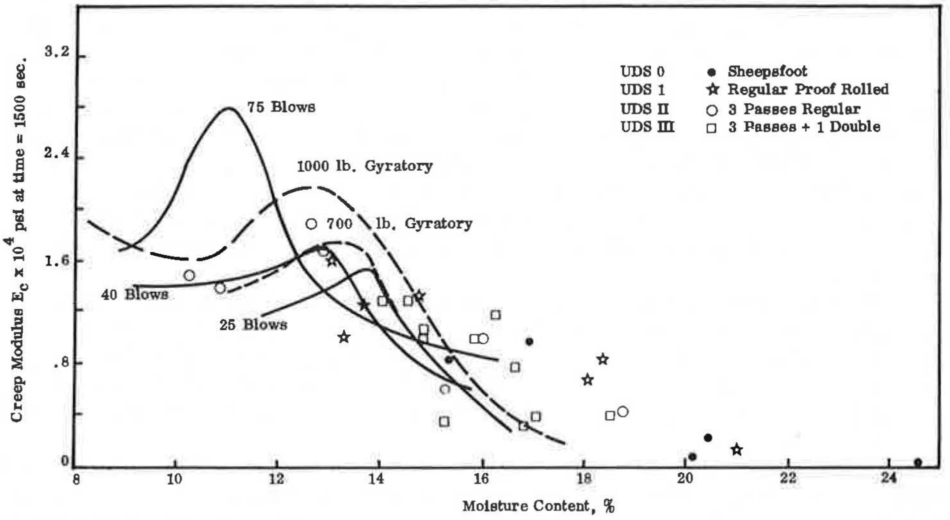

Figure 4. Creep moduli versus moisture content with various compaction methods.

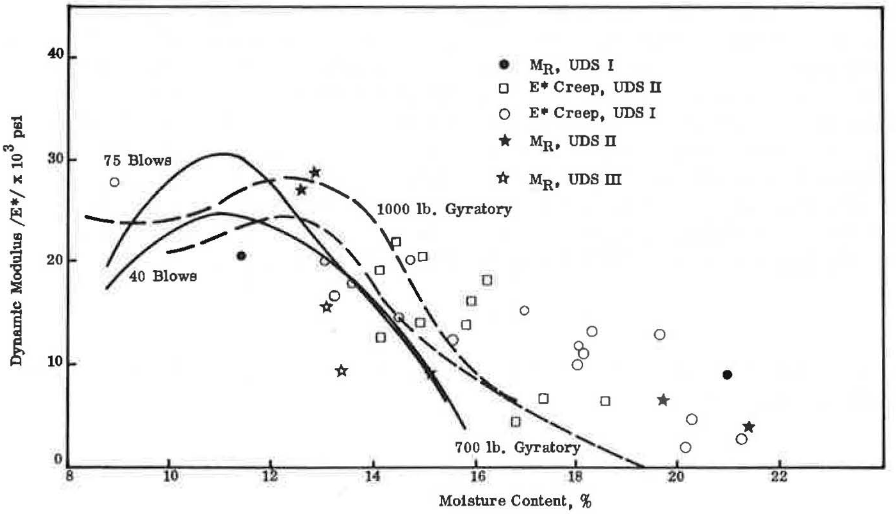

The variations of M_R with repeated load magnitude and confining stress are shown in Figure 5. The confining stresses were 0, 9, and 21 psi. The effect of confining pressure seems to be to shift the curve to the right, but the shape remains the same. The shape of the curves strongly suggests the existence of different phenomena at low and high stress levels. Figure 6 shows the variations of M_R with dynamic stress for unconfined experiments and for N = 30 and 3,000 cycles. M_R increases with an increase in dynamic stress up to a point and then decreases. Because there is little distinction between N = 30 and N = 3,000 at low stress levels, densification or work-hardening phenomena are apparently occurring. At higher dynamic stresses, however, the substantial difference between N = 30 and N = 3,000 cycles suggests a damage or work-softening phenomenon. Obviously the greater the number of load cycles is, the lower the modulus of resilience will be.

Of the above findings, the variation of M_R with the magnitude of the applied stress is of particular significance. Seed et al. (35) investigated deviator stresses ranging from 3.1 to 50 psi (representing about 5 and 80 percent of the ultimate strength of the samples) and reported values of M_R for N = 200 and 100,000. Their results showed M_R to decrease rapidly and then increase at a very slow rate as stress was increased. No explanations were offered for that behavior.

In this study, deviator stresses varying from 22 to 126 psi (representing 12 to 68 percent of the ultimate strength) were used, and values of M_R are reported at N = 1,000 and 3,000. There was agreement between this study and that of Seed et al. (35) in that they both indicated a range of stresses over which M_R increased and then decreased gradually. For unconfined experiments, however, this study showed that the values of M_R increased with stress under the endurance limit.

Figure 7 shows the relation of resilient modulus with the ratio of applied stress to ultimate strength for confining pressures of 0, 9, and 21 psi in triaxial tests. The general shape of the curve is very similar to that shown in Figure 6. However, the data are superimposed in a single master curve irrespective of confining pressure. Furthermore, the first branch of the M_R-σ relation corresponding to the densification or work-hardening phenomena is apparently only occurring under unconfined experiments. Because subgrade soil elements under pavement structure are under confining pressure, it appears that the second branch of M_R-σ (i.e., the work-softening branch) is of more practical value. That observation is in accordance with the findings of Seed et al. (35). The M_R-σ relation can in general be expressed approximately by

$$M_R = B\,\theta^{-m}$$

where B and m are constants, and θ is a stress invariant ($\theta = \sigma_1 + \sigma_2 + \sigma_3$). This relation can also be expressed approximately by

$$M_R = B_1\left(\frac{\sigma_{dynamic}}{\sigma_{ultimate}}\right)^{-m_1}$$

where B_1 and m_1 are material constants, and $\sigma_{ultimate}$ is compressive strength determined in triaxial tests.

ULTIMATE RESPONSE

Compressive Strength

The factors influencing the shear strength of a subgrade soil are moisture content at compaction, moisture changes after compaction, dry density, and soil structure. Moisture has a very significant effect on the performance of clay subgrade soil. Taken in combination with compactive effort and type of compaction, it determines the resulting dry density and more important the soil structure (35, 36, 37). Soil structure is an important presage of soil behavior. For the same values of moisture content and dry density, the stress-strain curve for a soil with a flocculated structure is much steeper and has a different shape than that for the same soil with a dispersed structure.

Figure 5. Variation of M_R with stress invariant.

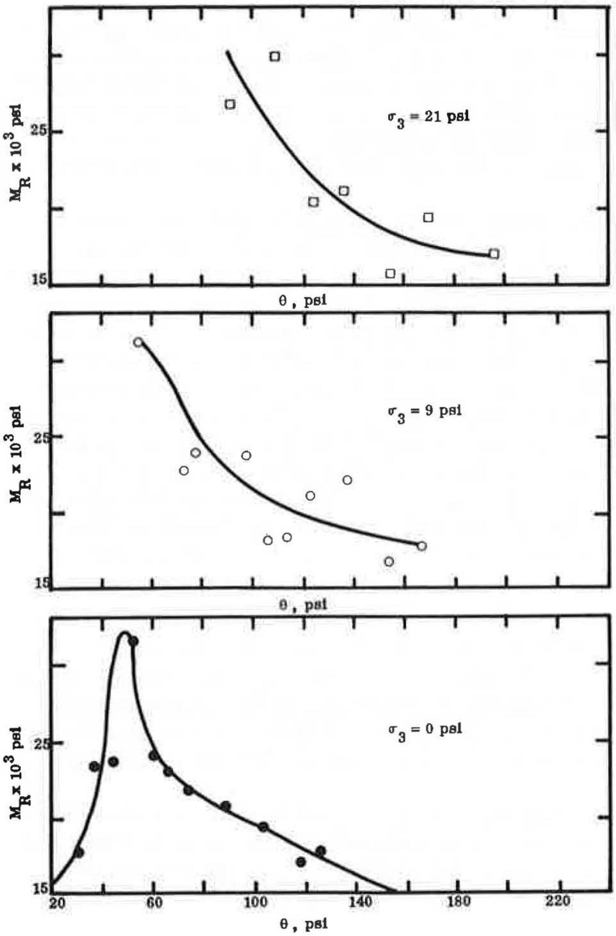

Figure 6. Variation of M_R with stress level after 30 and 3,000 cycles of load repetition.

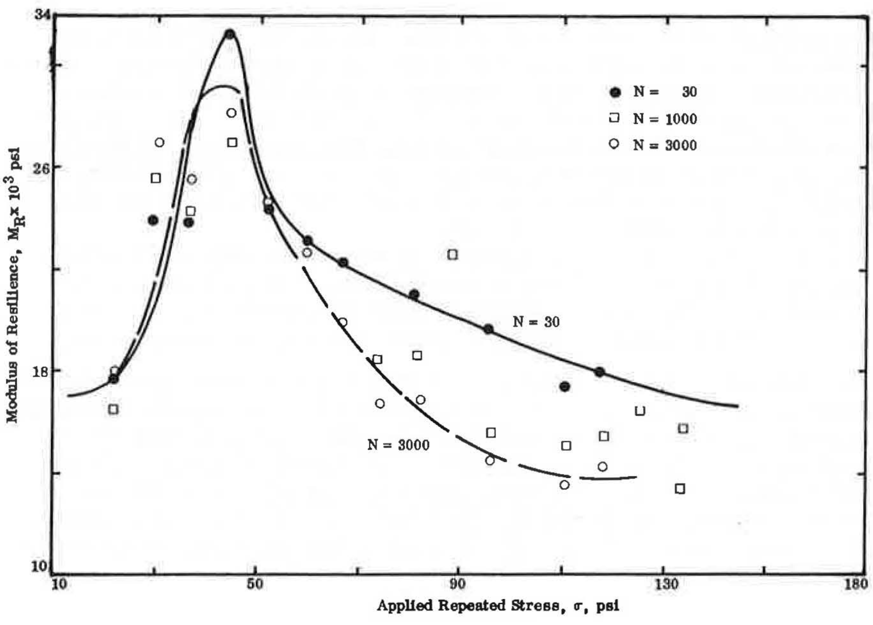

Comparisons of the unconfined compressive strength of 700- and 1,000-lb gyratory-compacted specimens at various moisture contents (Fig. 2) show that the difference in the shear strength for specimens compacted on the wet side of optimum is rather small. That is obviously attributed to the dispersed structure formed at high moisture contents. The difference in the shear strength, however, becomes larger as specimens having less moisture content (i.e., compacted on the dry side of optimum) are compared.

Similarly, the difference in the unconfined compressive strength of drop-hammer-compacted soils on the wet side of optimum is rather small. The fact that all specimens attain approximately similar strength characteristics at moisture contents greater than 15 percent, despite their differences in dry density, again points to the overriding influence of structure on strength. However, for specimens compacted on the dry side of optimum by drop-hammer compaction, the influence of compactive energy on the strength is more pronounced. That is, the increase in the compactive energy results in a greater increase in the unconfined compressive strength. If the strength-moisture content relations are considered, the drop-hammer-compacted specimens are more sensitive to moisture variation than gyratory-compacted specimens. This again points to the differences in the structure of compacted clay as affected by the method of compaction. Finally, it is clearly noted that the unconfined compressive strength of field specimens agrees very closely with the results of gyratory-compacted specimens.

Cumulative Deformation: Rutting

Studies of elastomers, metals, and asphalts have shown that the cumulative-deformation and failure response of materials under repeated loading are very similar to that of the creep-rupture phenomena. It has been asserted that the principles of static and dynamic rupture are identical and that the observed difference in the life of specimens is due to the rate of cumulative damage and relaxation between load applications.

Figure 8 shows a typical deformation-time relation for a soil specimen under repeated loading in which the variation of cumulative permanent deformation γ_p with number of load applications is presented. It is noted that, similar to creep-rupture phenomena, the cumulative permanent deformation-time relation might be divided into 3 distinct stages:

1. Initially the deformation increases rapidly but with a decreasing rate with the number of cycles of loading. Densification may occur here and involves the decrease in air-void content of the soil by the progressive rearrangement of the particles relative to each other.
2. The second stage involves the time-dependent rearrangement of the particles. It is an irrecoverable flow process and is effected by the successive yielding and deformation of particle contacts. The resultant deformation response during this state is in accordance with the postulates of the rate process theory; the rate of permanent deformation is expressed in terms of the number of load applications instead of the time of load applications. The rate of deformation and volume change are considerably reduced, consistent with the idea of a flow of particles into the vacated voids and rearrangement as opposed to a translation of particles.
3. The third stage is characterized by an increase in the rate of deformation leading ultimately to failure. Failure is due to an accumulation of damage resulting from the formation and growth of plastic zones at points of local overstressing and the enlargement of voids and weak boundaries in the soil structure under repeated loading.

In this study, the rate process theory concepts are used to explain the accumulation of permanent deformation of stages 1 and 2 for clay specimens under repeated loadings.

The theory of absolute reaction rates or rate process theory, proposed initially by Eyring et al. (15) and applicable to processes involving the motion of particles, has been used extensively to describe and predict the creep and consolidation behavior of clays as well as other materials (16, 17, 18, 19, 20, 21, 22, 23, 24, 25). The contributions of Mitchell, Campanella, and Singh (21, 27) in adapting the theory of absolute reac-

Figure 7. Variation of M_R with stress ratio for different confining pressures.

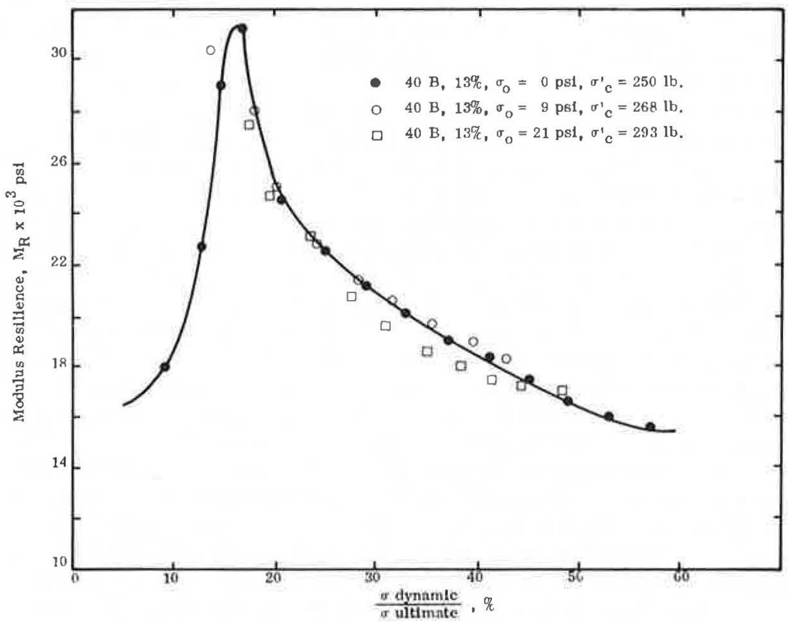

Figure 8. Typical deformation-load cycle curve.

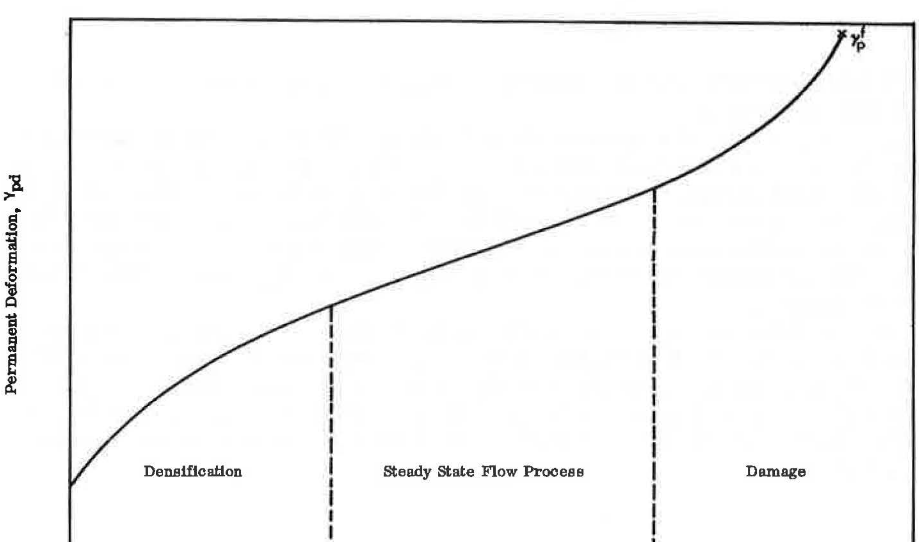

tion rates to the study of the time-dependent deformation of soils have been especially significant. The most significant aspect of their work is the recognition of the fact that "structure" can affect the time response of soils, and they have accordingly adapted the general rate process equation by the inclusion of a parameter to account for this influence. The work by Mitchell et al. forms the basis for this investigation into the mechanism of the deformation of clay soil subjected to repeated loading.

Mitchell et al. (21), working with clay soil under static creep loading, observed that plots of axial strain versus time on a log-log scale gave parallel lines for different stress levels, which indicated an independence between creep stress and slope. The slope is negative, however, meaning that for any given stress the creep rate decreases in a regular manner with time. Similar observations were made in this study. Figure 9 shows a plot of ln ($d\gamma_{pd}/dN$) versus ln N; the interrelation among $d\gamma_{pd}/dN$, N, and repeated stress is similar to that among $d\gamma/dt$, t, and creep stress under static loading conditions. That similarity in observed response leads to the obvious conclusion that the mechanisms of compacted clay deformation under static and dynamic conditions are very similar, if not the same. The possibility exists, therefore, of being able to predict dynamic response from static tests and vice versa. The term γ_{pd} used in this analysis denotes the deviatoric component of permanent deformation. In this investigation, in accordance with soil mechanics conventions, stress and strains are resolved into components responsible for change of volume and those responsible for change of shape. Because the flow process is essentially a constant volume process, the rate process is then applied to only the deviatoric component of permanent deformation γ_d.

The nature of the observed interrelations between ln ($d\gamma_{pd}/dN$) and ln N at constant repeated stress σ (Fig. 9) and between ln ($d\gamma_{pd}/dN$) and σ at constant N (Fig. 10) suggests that the deformation rate of compacted clay under stresses that are not large enough to cause accelerated damage may well be expressed by the following equation:

$$\frac{d\gamma_{pd}}{dN} = A\, e^{B\sigma}\, N^{D}$$

where A and B are constants, and D is stress dependent. A, however, may be both structure and time dependent.

As mentioned before, the rate process theory concepts apply to primary and secondary stages of the deformation-time relation. For the third stage, McClintock (32, 33) has indicated that, once damage is initiated, a plastic zone extends a distance R in front of the overstressed region. As a first approximation, it might be assumed that failure depends only on the strain and that failure will occur whenever the strain reaches a critical value. This critical plastic strain at failure is called γ_p^f, which represents the critical level of damage.

Besides the cumulative damage rule and the critical magnitude of damage occurring at the event of failure γ_p^f, the rate of damage accumulation under repeated load application is of theoretical interest. In analogy to the processes of deformation, damage growth associated with cracking, and reaction rate principles describing bond breakage and deformation, Guirguis (34) has proposed an empirical power law for the damage growth equation given as

$$\frac{d\gamma_p}{dN} = c\, (\gamma_p)^{m}$$

where

- γ_p = plastic deformation at any time of loading,
- N = number of cycles,
- c = soil constant, and
- m = constant independent of the stress level.

He found m ranged from 8 to 11 for various soils compacted at optimum moisture content and used a range of stress levels and compaction energies (Figs. 11 and 12).

Figure 9. $d\gamma_{pd}/dN$ versus N (log-log scale).

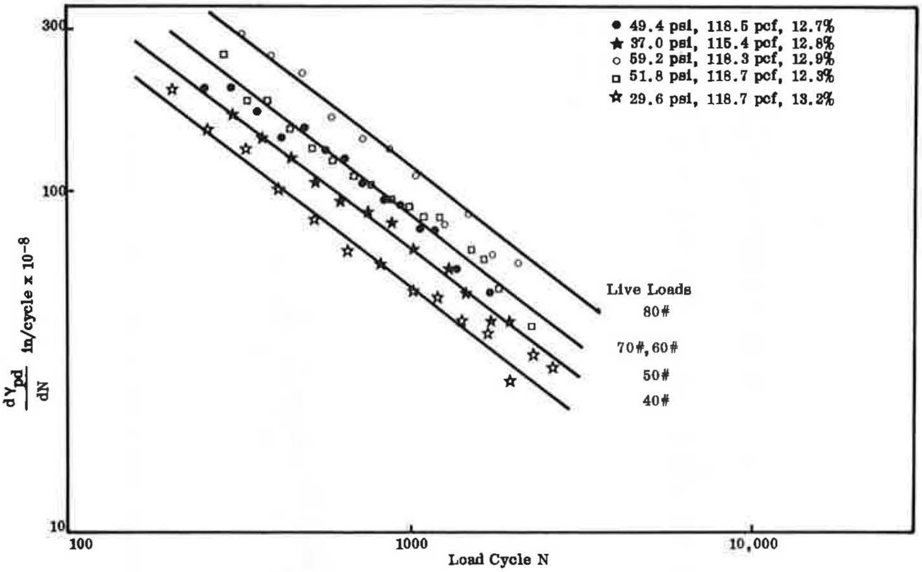

Figure 10. $d\gamma_{pd}/dN$ versus p_d for 40-blow compaction.

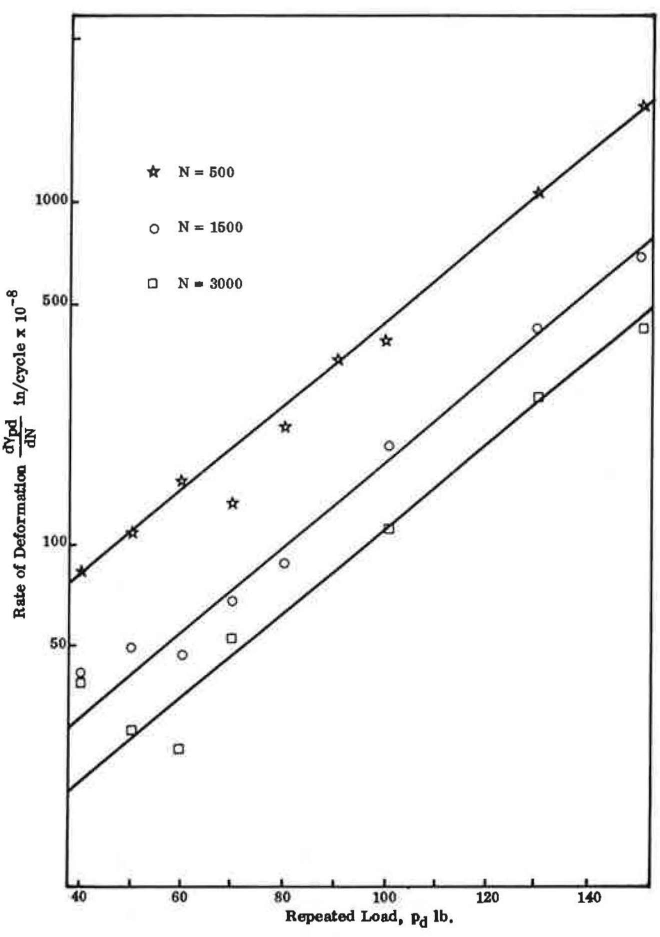

Figure 11. $d\gamma_{pd}/dN$ versus γ_{pd} for 40-blow compaction (log-log scale).

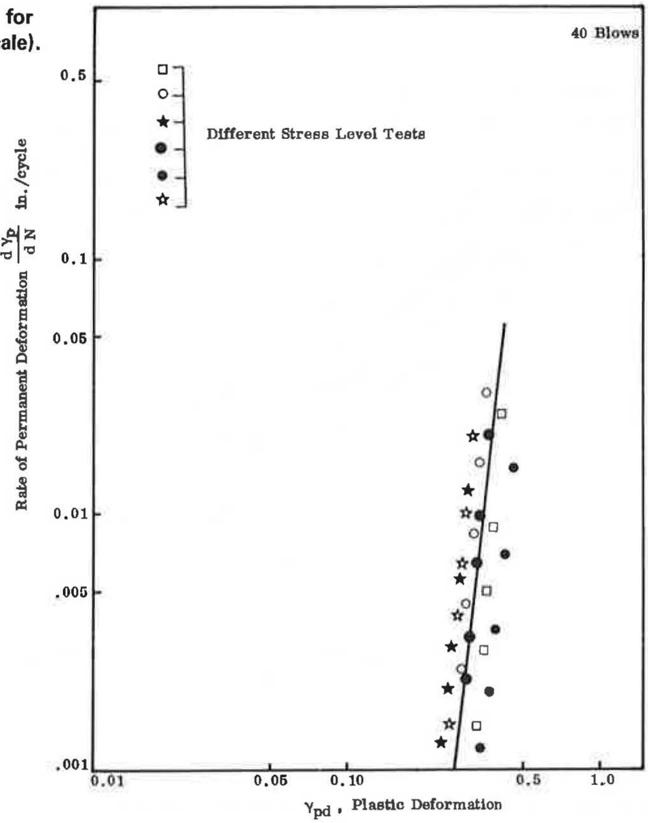

Figure 12. $d\gamma_{pd}/dN$ versus γ_{pd} for the average of various compaction methods.

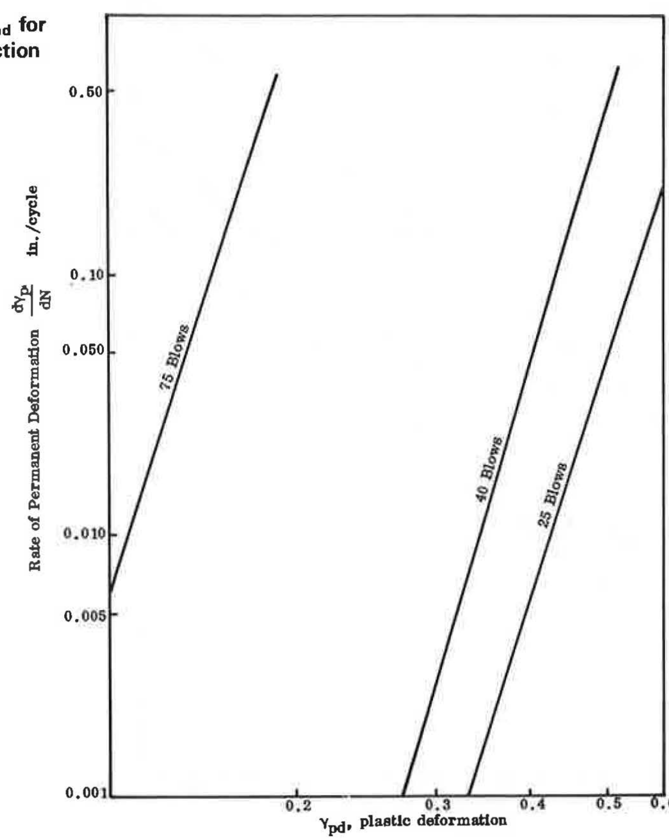

It can be easily shown that such a power law relation between the rate of permanent deformation and the magnitude of the permanent deformation itself exists during the entire repeated-loading deformation process up to failure. During densification and steady-state flow, however, the power law equation has a negative index; during the damage branch, the index changes signs. The point of transition of those lines gives the magnitude of permanent deformation at which the damage rate becomes critical. This suggests an additional criterion for pavement subgrade design: For the subgrade material and stress conditions anticipated in service, the permanent deformation must not exceed a certain critical value γ_p^c (can be assumed to be 0.70 γ_p^f). The design problem would then be to determine the value of γ_p^f for a given subgrade material and to predict the number of load applications N required to bring about γ_p^c. The signs are optimistic that this can be done.

SUMMARY AND CONCLUSIONS

This research has been carried out primarily to study the correlation between engineering and physical properties of field- and laboratory-compacted subgrade specimens. In addition, other fundamental material characteristics that best describe the subgrade performance have also been presented. The conclusions derived from this study are given below:

1. The 1,000-lb gyratory, the 40-blow drop-hammer, the undisturbed field samples, and the Ohio Department of Highways (curve K) compaction curves agree with each other.
2. Shear strength characteristics of undisturbed field samples and 700-lb gyratory laboratory samples agree very well.
3. The compaction of creep modulus E_c and moisture content relation of 700-lb gyratory, 40-blow laboratory samples, and undisturbed field samples agree closely. The maximum creep modulus occurs at the optimum conditions of density and shear strength.
4. The dynamic modulus $/E^*/$ determined from the transformation of creep data has the same trend as E_c.
5. The resilient modulus M_R decreases as the number of load applications N increases for stresses above the endurance limit, that is, stresses large enough to cause damage. For stresses less than the endurance limit, M_R increases as N increases for the range of values of N investigated (3,600 maximum). The results also indicate that the resilient modulus M_R varies with the magnitude of the repeated load and the ratio of applied load to strength and is expressed as follows:

$$M_R = B_1 \left(\frac{\sigma_{dynamic}}{\sigma_{ultimate}} \right)^{-m_1}$$

It is also noted that M_R and $/E^*/$ show close agreement.

6. It has been shown that, for deviatoric permanent deformation, the branches of densification and steady-state flow of the γ_{pd}-N relation are in accordance with the postulates of the rate process theory and can be expressed as

$$\frac{d\gamma_{pd}}{dN} = A\, e^{B\sigma}\, N^D$$

where D is a stress-dependent constant. It has also been shown that the damage branch of the same relation can be expressed as a power law

$$\frac{d\gamma_p}{dN} = c\, (\gamma_p)^m$$

where m = 8→11. Furthermore, the data indicated that failure occurs when accumulated permanent deformation reaches a constant value γ_p^f, which has been found to be independent of the path taken to failure.

REFERENCES

1. An Outline of Suggestions for Study of Compaction of Earthwork. Highway Research Correlation Service, May 1964.
2. Symposium on Compaction of Earthwork and Granular Bases. Highway Research Record 177, 1967.
3. Soil Compaction and Proof-Rolling of Subgrades. HRB Bull. 254, 1960.
4. Compaction of Soils. ASTM, Spec. Tech. Publ. 377, June 1964.
5. Seed, H. B., and Chan, C. K. Undrained Strength of Compacted Clays After Soaking. Jour. Soil Mech. and Found. Div., Proc., ASCE, Oct. 1959, pp. 31-47.
6. Seed, H. B., Mitchell, J. K., and Chan, C. K. The Strength of Compacted Cohesive Soils. Proc., ASCE Res. Conf. on Shear Strength of Cohesive Soils, 1960, pp. 877-964.
7. Seed, H. B., and Chan, C. K. Structure and Strength Characteristics of Compacted Clays. Jour. Soil Mech. and Found. Div., Proc., ASCE, Oct. 1959.
8. Mitchell, J. K., Hooper, D. R., and Campanella, R. G. The Permeability of Compacted Clays. Jour. Soil Mech. and Found. Div., Proc., ASCE, July 1965.
9. Pagen, C. A., and Jagannath, B. N. Fundamentals of Soil Compaction. Eng. Exp. Station, Ohio State Univ., Rept. EES 248-1, July 1966.
10. Pagen, C. A., and Jagannath, B. N. Effect of Gyratory Compaction on the Rheological Characteristics of Clay. Eng. Exp. Station, Ohio State Univ., Rept. EES 248-3, 1966.
11. Pagen, C. A., Wang, C., and Jagannath, B. N. Effect of Compaction and Increase of Saturation After Compaction on the Engineering Properties of Compacted Clay. Eng. Exp. Station, Ohio State Univ., Rept. EES 248-6, July 1968.
12. Pagen, C. A., and Khosla, V. K. Frost Action Characteristics of Compacted Cohesive Soil. Eng. Exp. Station, Ohio State Univ., July 1968.
13. Pagen, C. A., and Jagannath, B. N. Resilient and Residual Mechanical Properties of Compacted Kaoline Clay. Eng. Exp. Station, Ohio State Univ., July 1968.
14. Pagen, C. A., and Jagannath, B. N. Rheological Properties of Hybla Valley Clay. Eng. Exp. Station, Ohio State Univ., July 1969.
15. Glasstone, S., Laidler, K., and Eyring, H. The Theory of Rate Process. McGraw-Hill, New York, 1941.
16. Abdel-Hady, M., and Herrin, M. Characteristics of Soil-Asphalt as a Rate Process. Jour. Highw. Div., Proc., ASCE, Vol. 92, No. HW1, March 1966.
17. Andersland, O. B., and Akili, W. Stress Effect on Creep Rates of a Frozen Clay Soil. Geotechnique, Vol. 17, March 1967.
18. Christensen, R. W., and Wu, T. H. Analysis of Clay Deformation as a Rate Process. Jour. Soil Mech. and Found. Div., Proc., ASCE, Vol. 90, No. SM6, Nov. 1964.
19. Herrin, M., and Jones, G. The Behavior of Bituminous Materials From the Viewpoint of the Absolute Rate Theory. Proc., AAPT, Vol. 32, Feb. 1963.
20. Herrin, M., Marek, C. R., and Strauss, R. The Applicability of the Absolute Rate Theory in Explaining the Behavior of Bituminous Materials. Proc., AAPT, Vol. 35, Feb. 1966.
21. Mitchell, J. K., Campanella, R., and Singh, A. Soil Creep as a Rate Process. Jour. Soil Mech. Div., Proc., ASCE, Vol. 94, No. SM1, Jan. 1968.
22. Mitchell, J. K. Shearing Resistance of Soils as a Rate Process. Jour. Soil Mech. and Found. Div., Proc., ASCE, Vol. 90, No. SM1, Jan. 1964.
23. Murayama, S., and Shibata, T. Rheological Properties of Clays. Proc., 5th Int. Conf. Soil Mech. and Found. Eng., Paris, 1961.
24. Singh, A., and Mitchell, J. K. General Stress-Strain-Time Function for Soils. Jour. Soil Mech. and Found. Div., Proc., ASCE, Vol. 94, SM1, Jan. 1968.
25. Wu, T. H., Resendiz, D., and Neukirchner, R. J. Analysis of Consolidation by Rate Process Theory. Jour. Soil Mech. and Found. Div., Proc., ASCE, Vol. 92, No. SM6, Nov. 1966.
26. Murayama, S., and Shibata, T. On the Rheological Characteristics of Clay—Part I. Disaster Prevention Res. Inst., Kyoto Univ., Japan, Bull. 26, 1958.
27. Mitchell, J. K., Singh, A., and Campanella, R. Bonding, Effective Stresses and Strength of Soils. Jour. Soil Mech. and Found. Div., Proc., ASCE, Vol. 95, No. SM5, Sept. 1969.

28. Christensen, R. W., and Kim, J. S. Rheological Model Studies in Clay. Dept. Eng. Mech., Univ. of Wisconsin, Madison, 1969.
29. Polakowski, N. H., and Ripling, E. J. Strength and Structure of Engineering Materials. Prentice-Hall, New Jersey, 1966.
30. Fletcher, T. A. Fatigue Analysis of a Sand-Asphalt Mixture. Ohio State Univ., MS thesis, 1968.
31. Bartenev, G. M., and Zuyev, Yu. S. Strength and Failure of Viscoelastic Materials. Pergamon Press, New York, 1968.
32. McClintock, F. A., and Argon, A. S. Mechanical Behavior of Materials. Addison-Wesley, 1966.
33. McClintock, F. A. On the Plasticity of the Growth of Fatigue Cracks. In Fracture of Solids, John Wiley and Sons, New York, 1962.
34. Guirguis, H. R. Subgrade Compaction and Its Performance Under Traffic Loads. Ohio State Univ., MS thesis, 1970.
35. Seed, H. B., Chan, C. K., and Lee, C. E. Resilience Characteristics of Subgrade Soils and Their Relation to Fatigue Failures in Asphalt Pavements. Proc., Int. Conf. Struct. Des. of Asphalt Pavements, Univ. of Michigan, Aug. 1962.
36. Lambe, T. W. The Structure of Compacted Clay. Jour. Soil Mech. and Found. Div., Proc., ASCE, Vol. 84, No. SM2, 1958.
37. Langfelder, L. J., and Nivargikar, V. R. Some Factors Influencing Shear Strength and Compressibility of Compacted Soils. Highway Research Record 177, 1967, pp. 4-21.

TEMPERATURE EFFECT ON IRREGULARLY SHAPED COMPACTION CURVES OF SOILS

Peter Y. Lee and D. C. Hsu, Department of Civil Engineering, South Dakota State University

ABRIDGMENT

•THIS investigation is the third stage of a series of investigations to examine the characteristics of irregularly shaped compaction curves. Because the change of temperature is an important factor in influencing the engineering properties of soil and prior research on temperature effect only examined the single-peak compaction curve, this paper attempts to investigate carefully the effect of temperature on the irregularly shaped compaction curve. Some investigations concerning the characteristics of irregular compaction curves were performed by Lee and Suedkamp (1). After investigating 34 different soils with the standard AASHO compaction test, they found that on the modified Casagrande's classification scheme there are 2 approximate regions that show irregularly shaped compaction curves. The soils with liquid limits greater than 70 and less than 30 usually create irregularly shaped compaction curves. On the other hand, the soils with liquid limits between 30 and 70 produce single-peak curves. Lee and Suedkamp also indicated that 4 types of curves exist: a typical single-peak compaction curve, a 1½-peak curve, a double-peak curve, and an oddly shaped curve.

The importance of temperature on the compaction curves has so far been given little consideration. Johnson and Sallberg (2) found, primarily from a search of the literature, that increasing the temperature leads to an increase of the maximum dry density of the single-peak curve. They explained that the water in the soil is more viscous at the lower temperature, reducing the workability of the soil and inducing a lower dry density. Some investigations that were not involved in the compaction tests have shown the temperature effect on some soil properties (3, 4, 5, 6, 7, 8). Sherif and Burrous (3) concluded that an increase in the temperature causes a decrease in the shearing strength of the soil. That conclusion is in agreement with most other investigations, although not all indicate exactly the same results.

LABORATORY INVESTIGATION

Preparation of Soil

A description of the selected samples is given in Table 1. The samples represented a wide range of engineering characteristics as well as compaction curves of soils. In addition to the combinations of known minerals, some natural soils were chosen to be examined.

Each time the soils were air-dried and pulverized to pass a No. 4 sieve, they were mixed with water in increments of 2 or 3 percent. Every sample was put into a leak-proof plastic bag. A batch of samples was sealed in a big plastic bag and stored in a moisture control room for at least 24 hours.

Apparatus and Test Methods

The specimens were tested at 40, 80, and 120 F with ±5 F deviation. To control the temperature, a thermal-insulated chamber was built with plywood and insulation to surround the standard compactor (Fig. 1). A deep freezer was connected to the right side of the insulated chamber to hold the cool air at 40 F. The higher temperatures were provided by a heater with a thermostat that ranged from 70 to 140 F.

The samples, which had been stored in the moisture control room, were deposited in the chamber under the desired temperature for more than 12 hours before testing.

Standard AASHO Designation T 99-70 Method A (also indicated as ASTM Designation D698-70 Method A) was the primary method applied in this research.

RESULTS AND ANALYSIS

Lower Water Content

At the lower water content, the temperature seems to have no significant influence on the compaction curves, and data of various temperatures show no consistent relation. There are some reasons that can explain this pehnomenon.

The increase in dry density of the compaction curve due to increasing temperature is attributed to the increase in pore pressure. However, the pore pressure essentially has a negligible effect on the 1½-peak compaction curve of pure sand (soil 1, Fig. 2). Therefore, the compaction curve of pure sand is only negligibly affected by temperature. For the double-peak curve in the lower region (liquid limit <30), despite the fact that the pore pressure is an important factor in the shaping of the compaction curve (1), some other factors are involved causing the random results with water content from 0 to 7 percent (soil 2, Fig. 3). Also, for 1 natural soil (soil 8, liquid limit = 30, plasticity index = 25), the increase of temperature had no significant influence on the water content between 0 and 7.5 percent (Fig. 2). It must be pointed out here that other laboratory variables play a more dominant role than temperature, particularly for the more sensitive fine-grained soil containing a small amount of water. Thus, the results reflect the effect of the uncertainty due to laboratory variables rather than to the effect of temperature. For instance, when the compaction ram dropped onto the fine-grained soil with lower water content, the force of the compaction ram expelled the fine soil particles out of the mold as dust; thus, the accuracy was reduced. Even though these factors influence the data accuracy, they do not significantly change the shape of the compaction curve. Results show that those samples (liquid limit >70, Fig. 4), whose water content ranges from 0 to about 15 percent, behave as randomly as the samples selected from the lower region (liquid limit <30). It is known that the highly cohesive soils are very difficult to mix evenly with water, especially at the lower water content. Because water plays an important part in the compaction process, the uneven distribution of water, in addition to the variable factors discussed above, will also affect the oddly shaped compaction curves. Therefore, the resulting data are quite scattered.

Higher Water Content

When more water is added, the temperature starts to reveal some effects on the compaction curves, although the effect is not clearly apparent on the 1½-peak curve of pure sand (Fig. 2). For soils with a liquid limit <30 and water content from about 7 percent to optimum point (soil 8, Fig. 2 and soil 2, Fig. 3) and soils with liquid limit >70 and water content from about 15 percent to saturation point (Fig. 4), the increasing temperature tends to increase the dry density. An increase in temperature decreases the viscosity of water and expands the electric double layers of soil particles, thereby producing a greater dry density. Essentially, one of the predominant factors is that the increasing temperature reduces the rigid state of water that surrounds the individual soil particles, increasing the pore pressure. Increasing pore pressure is associated with decreasing effective shear strength, which allows the soil particles to slide closely to each other and results in a higher dry density. Some of those highly cohesive clays in the portion of higher water content, for instance, soil 4, still show some scattered data, and others, e.g., soil 5 (Fig. 5), show some well-distributed data. The reason is that pore pressure is only a part of the influence on the shape of oddly shaped compaction curves, and the most logical explanation would be to consider the physicochemical characteristics of the minerals present (1). The temperature effect on the wet side of the compaction curve decreases for all soils.

Table 1. Selected soil samples.

Sample	Sand[a] (percent)	Montmoril-lonite[b] (percent)	Illinite[c] (percent)	Kaolinite[d] (percent)	Liquid Limit	Plasticity Index
1	100	0	0	0	0	NP
2	75	0	0	25	13	NP
3	0	0	100	0	51	21
4	50	50	0	0	230	198
5	25	50	25	0	172	142
6	0	50	50	0	170	129
7	0	25	50	25	105	73
8[e]					30	25
9[e]					72	32

[a]Pure sand obtained locally.
[b]Bentonite obtained from Baroid Div. of Nat. Lead Co., Houston.
[c]Grundite obtained from Green Refractionery Co., Morris, Illinois.
[d]Clay Hydrite-121 obtained from Thompson-Hayward Chemical Co., Kansas City, Kansas.
[e]Natural soil.

Figure 1. Test setup.

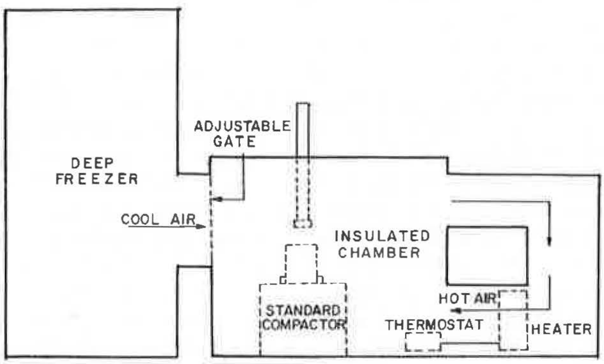

Figure 2. 1½-peak curve showing effects of temperature.

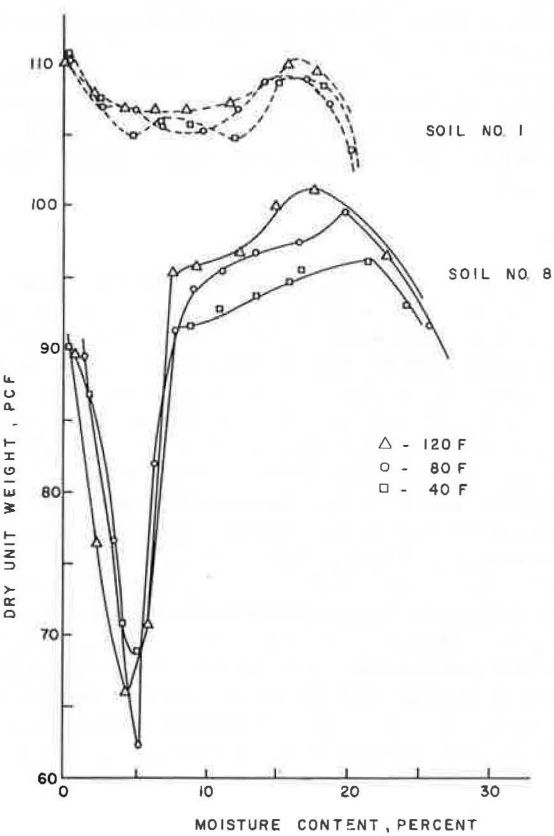

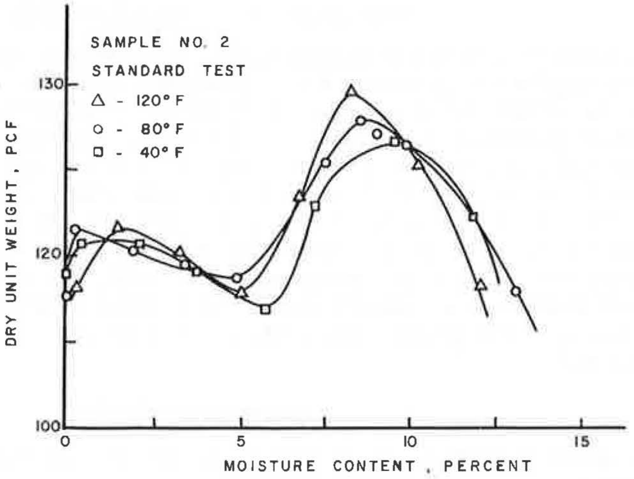

Figure 3. Double-peak curve showing effects of temperature.

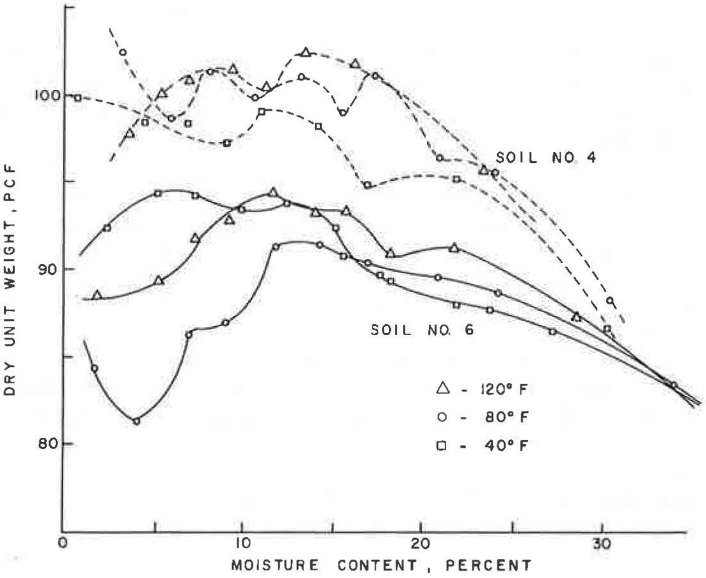

Figure 4. Oddly shaped curve showing effects of temperature on soils 4 and 6.

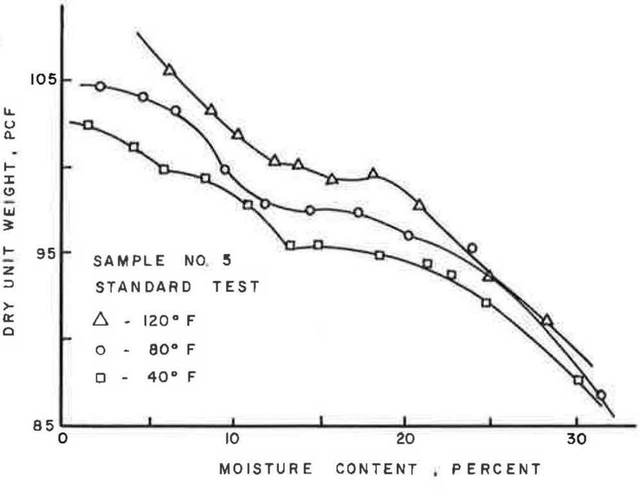

Figure 5. Oddly shaped curve showing effects of temperature on soil 5.

SUMMARY AND CONCLUSIONS

On the basis of a series of temperature-controlled experimental tests, several conclusions can be established. The investigated variation in temperature produces no significant influence for all the soils at the lower water content. The range of water content showing negligible temperature effects is from 0 to 7 percent for soils with a liquid limit <30 and from 0 to about 15 percent for soils with a liquid limit >70. Temperature has a negligible effect on the $1\frac{1}{2}$-peak compaction curve of sandy soil that has an extremely low liquid limit. For soils with a liquid limit <30 and a water content from about 7 percent to the optimum point and soils with a liquid limit >70 and a water content from about 15 percent to the saturation point, the increasing temperature results in an increase of dry density because the higher temperature is associated with lower strength. This phenomenon tends to decrease after the saturation moisture content is reached.

ACKNOWLEDGMENTS

The financial support provided by the National Science Foundation is gratefully acknowledged.

REFERENCES

1. Lee, P. Y., and Suedkamp, R. J. Characteristics of Irregularly Shaped Compaction Curves. Highway Research Record 381, 1972, pp. 1-9.
2. Johnson, A. W., and Sallberg, J. R. Factors Influencing Compaction Test Results. HRB Bull. 319, 1962, pp. 1-146.
3. Sherif, M. A., and Burrous, C. M. Temperature Effects on the Unconfined Shear Strength of Saturated, Cohesive Soil. HRB Spec. Rept. 103, 1969, pp. 267-272.
4. Plum, R. L., and Esrig, M. I. Some Temperature Influences on Soil Compressibility and Pore Water Pressure. HRB Spec. Rept. 103, 1969, pp. 231-242.
5. Campanella, R. G., and Mitchell, J. K. Influence of Temperature Variations on Soil Behavior. Jour. Soil Mech. and Found. Div., Proc. ASCE, Vol. 95, No. SM3, 1968, pp. 709-734.
6. Mitchell, J. K. Shearing Resistance of Soils as a Rate Process. Jour. Soil Mech. and Found. Div., Proc. ASCE, Vol. 90, No. SM1, 1964.
7. Seed, H. B., Mitchell, J. K., and Chen, C. K. The Strength of Compacted Cohesive Soils. Proc., ASCE Res. Conf. on Shear Strength of Cohesive Soils, 1960, pp. 877-964.
8. Laguros, J. G. Effect of Temperature on Some Engineering Properties of Clay Soils. HRB Spec. Rept. 103, 1969, pp. 186-193.

ACCEPTANCE SPECIFICATION OF COMPACTED SOILS

Leland M. Kraft, Jr., McClelland Engineers, Inc.; and
Jimmy Yew-Hang Yeung, Case Western Reserve University

An investigation of the failure probability of linear elastic heterogeneous embankments is reported, and illustrations are given for incorporating those results into acceptance specifications. Failure is defined in terms of deformations. Uncertainties in the soil stiffness include the spatial uncertainty and the uncertainty resulting from limited sampling during the inspection process. The results give a quantitative measure of the failure probability as influenced by the embankment height and slope angle, the slope geometry, the mean and standard deviation of the soil stiffness, Poisson's ratio, the number of samples taken during the inspection, and the mean and standard deviation of the measurements taken during the inspection. A hypothetical problem illustrates the use of the results, which can be tabulated for easy field use. The influence of neglecting the spatial uncertainty of the soil properties in acceptance requirements is also illustrated.

• ONE PURPOSE of compaction specifications is to provide assurance that the properties of the compacted soil comply with the values of the design. If the strength or stiffness of the compacted soil is less than the design value, a failure is more likely to result. On the other hand, if the strength or stiffness of the compacted soil is greater than the design value, additional compaction effort and, thus, additional cost will be expended.

Even with very rigid product control, soil properties such as moisture and density vary from point to point within the compacted mass. The variation results from changes in the borrow material and changes in the placement conditions and is reflected by the compactive effort and environmental conditions. Extensive statistical data on moisture and density in compacted soil are readily available (2, 3, 12). An uncertainty in the soil properties also results from testing errors and incomplete sampling for product control. Decisions for accepting or rejecting a unit of compaction work must be made, however, on the basis of the imperfect information furnished by the sampling and testing data. In view of the uncertainties associated with the information available for making a decision, a rational criterion for accepting or rejecting a unit of work should be based on statistics and probable risks.

A contractor's risk arises from the possibility that an acceptable unit of work may be rejected. An owner's risk arises from the possibility that an unacceptable unit of work may be accepted. Both risks are dependent on the statistical parameters of the compacted soil, testing method, and associated costs of the risks. To evaluate the risks requires that a method for determining the performance of statistically heterogeneous earth structures be available. The purposes of this paper are to present, in terms of a failure probability, the deformation behavior of statistically heterogeneous earth embankments as represented by an elastic material and to show how that information can be incorporated into earthwork acceptance specifications. This paper is concerned with acceptance specifications and not with product control requirements. Product control is a separate subject. It is assumed in this paper that sufficient consideration has been given to product control requirements.

NOTATION

The notation used in later sections of this paper is defined as follows:

a = soil constant;
b = soil constant;

c = soil constant;
C_{VE} = coefficient of variation of E;
$\overline{E}^*$ = measured mean stiffness;
$\overline{E}_d$ = design mean stiffness;
$f(\cdot)$ = probability density function;
F_s = safety factor, in terms of deformations;
H = embankment height;
n = number of samples;
$\overline{E}$ = mean soil stiffness parameter;
$\overline{k}$ = dimensionless deformation parameter;
$P[\cdot]$ = probability;
P_f = failure probability;
P_{fm} = maximum permissible P_f;
s_u = undrained shear strength;
S_E = measured variance;
w = moisture content, percent;
$\overline{w}_d$ = design mean w;
$\overline{w}^*$ = measured mean w;
$\overline{x}$ = normalized variable;
z = normalized variable, student t distribution;
α = $S_E/\overline{E}_d$;
β = $\overline{E}_d/\overline{E}^*$;
β_c = critical;
δS = deformation;
$\delta\overline{S}$ = mean deformation;
γ = soil unit weight;
γ_d = soil dry density;
$\overline{\gamma}_d$ = design mean γ_d;
$\overline{\gamma}_d^*$ = measured mean γ_d;
σ_k = standard deviation of k; and
η = $\overline{E}/\overline{E}^*$.

PERFORMANCE MODEL

An understanding and a quantitative evaluation of the performance of an earth structure with statistically heterogeneous properties are required for the development of a meaningful and workable statistical acceptance specification. Consider the performance of the earth embankment shown in Figure 1. Although conventional practice is to evaluate the performance of an embankment by using safety factors based on limiting equilibrium analysis, it is likely that in the future more emphasis will be placed on estimates of deformations (5). That change in emphasis is made possible by the recent developments of numerical methods to analyze nonlinear stress-strain behavior. In view of the recent interest in the estimate of deformations, this paper will use deformations rather than stresses to define failure. The performance may be evaluated on the basis of the deformation of the embankment surface. Large displacements, which may constitute failure, at interior points of an embankment should be reflected by the displacements of the surface. Thus, only surface displacements are considered. The embankment is divided into a finite number of elements as shown. The magnitude of soil properties, such as strength and compressibility, may differ from element to element. In view of this unknown variation in the soil properties, the deformation at any point is unknown. However, the uncertainty in the deformation can be described in probability terms, as will be mentioned later.

Most statistical data on compacted soils are in terms of moisture content and dry density. For a given soil and compaction method, strength and compressibility parameters of the compacted soil can be related to the molded moisture content and dry density (8, 11). If this functional relation is known, the statistical characteristics of strength and compressibility can be derived from the statistical data on moisture and density. The coefficient of variation of the compressive shear strength of a compacted plastic clay was found to be 0.4, even though the coefficients of variation of moisture and density for compacted soils are typically on the order of 0.10 and 0.05 respectively (17). When the soil stiffness modulus is proportional to the soil strength, the coefficients of variation of the stiffness and strength are equal.

Statistical data on natural (as compared to compacted) soils indicate that the coefficient of variation of soil strength ranges between 0.2 and 0.6 (13, 17). Those values are restricted to what are referred to as "grossly uniform deposits" (9). Such deposits contain only one soil type. It is reasonable to assume that the coefficient of variation of compacted soil strength is of the same order as those of natural soil deposits. Hence, in this study, values for the coefficient of variation are taken to range from 0.3 to 0.6. That variation in soil properties includes both spatial variations and variations resulting from the testing method. At the present time sufficient knowledge is not available to separate those variations. If the testing variation and bias tendencies are known, they could be incorporated into the analysis with little additional effort.

The finite-element analysis and a simulation technique to account for the statistical variation of soil properties within the embankment can be used to estimate the variation of the deformation of any point within the compacted embankment. Further details on the method for generating these data are given by Kraft and Yeung (7). As an illustration, the variations of the mean deformation for different slope angles at selected locations on an embankment are shown in Figure 2. Although the coefficient of variation of the soil stiffness was 0.6, the maximum coefficient of variation of the embankment deformation was only 0.25. The indeterminancy of the earth mass tends to reduce the uncertainty in the deformation at locations where larger displacements occur as compared to the uncertainty of the soil stiffness (7).

A state of failure can be defined if the maximum deformation of the embankment surface exceeds some critical value. The magnitude of the critical deformation depends on factors such as the function of the earth structure and aesthetics. For the sake of argument and for the purpose of illustration, the critical deformation is taken as the mean design deformation times an appropriate safety factor F_s for a preselected location on the embankment, such as points 1 or 2 shown in Figure 2. Other locations for the critical deformation can be taken at the discretion of the engineer.

According to Gould and Dunnicliff (4), crest settlements of modern embankment dams on dense foundations are typically 0.2 to 0.6 percent of their height. Limiting shear strains within the embankment are in the range of 0.03 to 0.1 radian. Inclinometer deflection readings in dams that have performed satisfactorily are typically 0.01 radian. These values for limiting and observed deformations and strains may serve as first estimates of a design criterion based on deformations rather than limiting equilibrium.

It is recognized that soils possess neither linear nor elastic stress-strain characteristics. However, for the safety factors commonly used against shear failures, the shear stresses within the earth structure may be of magnitude where the assumption of linearity serves as a good first approximation. D'Appolonia, Poulos, and Ladd (1) have demonstrated that the initial settlement of footings supported by a bilinear elastic material depends on the elastic modulus, ultimate strength, and initial shear stress ratio. For safety factors against shear equal to approximately 2.0 and low initial shear stress ratios, which are typical of overconsolidated soils, the elastic theory can be used to calculate the initial settlement, even though the soil stress-strain curve is nonlinear. In view of the limited state of quantitative knowledge on the subject of this paper, it also seems logical that a linear model be examined before a more complex stress-strain relation is pursued that requires a much larger amount of computer time. The safety factor in terms of deformation would be smaller than the safety factor against a shear failure, as shown in Figure 3.

FAILURE PROBABILITY

An analytical evaluation of the failure probability of a compacted earth embankment will assist in making a decision to accept, reject, or perform additional sampling on a unit of work. If the mean stiffness parameter E and variance are known, the failure probability is the probability that the selected deformation will exceed the mean design deformation times the safety factor. If the deformation is normally distributed, the failure probability is

$$P_f = P(\delta < \delta \overline{F}_s \mid \overline{E}) = 1 - \int_{-\infty}^{\overline{x}} \frac{e^{-\frac{1}{2}x^2}}{\sqrt{2\pi}}\, dx = \int_{\infty}^{-\overline{x}} \frac{1}{\sqrt{2\pi}} e^{-\frac{1}{2}x^2}\, dx \qquad (1)$$

where $\overline{x} = \overline{k}\ [(F_s - 1)/\overline{k}]$, and σ_k is the standard deviation of the deformation parameter $\overline{k}$, which is a dimensionless parameter $(\overline{\delta}\,\overline{E}/H^2\gamma)$. The parameters $\overline{k}$ and σ_k depend on the slope geometry, slope angle, Poisson's ratio, and C_{VE}.

The use of the normal probability density function, at least as a first approximation, may be justified on the argument that the deformation at any point is the result of the sum and multiplicative mechanisms of the interactions of the elements. For coefficients of variation less than approximately 0.3, both the log normal and normal distributions are very similar. If the well-known "central limit theorem" is used, the multiplicative mechanisms would tend to be log normally distributed and the sum mechanisms would tend to be normally distributed. If the coefficient of variation is small, the normal probability density function could then be used to approximate the total effect of the sum and multiplicative mechanisms. Although exceptions may be found to this argument, it is the opinion of the authors that the normal distribution serves as a very good first approximation for the larger mean deformations, which are the ones of predominant interest. Also, an examination of the coefficient of skewness and the coefficient of peakedness of the deformations obtained from the simulation results suggests that a normal distribution is a reasonable distribution for this problem.

For purposes of illustration, the vertical deformation at the center of an earth embankment will be used to define a state of failure. For the trapezoidal and triangular embankments shown in Figure 4, the relation between the failure probability and the safety factor is shown in Figure 5 for different slope angles.

The results shown in Figure 5 are based on statistical estimates of the means and variance of the deformation, as obtained by Kraft and Yeung (7), who used finite elements and a simulation technique. For the purposes here, it is assumed that the statistical estimates are exact. The uncertainty in the mean $\overline{E}$ is usually larger than the uncertainty in the deformations resulting from the simulation process. The simulation results are based on 100 to 200 samples, whereas the mean soil property in the field for a given section of compaction is based usually on 10 or fewer samples. Therefore, the assumption that the statistical estimates are exact is considered to be reasonable.

For a given embankment height, a change in slope angle implies a change in $\overline{E}$ for a given safety factor. The safety factor can be altered by changing the slope angle and embankment height and by holding $\overline{E}$ constant. The results shown in Figure 5 demonstrate that the failure probability depends on C_{VE} and slope angle rather than solely on the safety factor. Hence, if the safety factor concept is to be used with a consistent reliability, the magnitude of the safety factor should be selected by giving some consideration to C_{VE}, Poisson's ratio, slope angle, and slope geometry for the particular job. The results shown in Figure 5 demonstrate that, for a given set of conditions, the triangular embankment is more reliable than the trapezoidal embankment. These results give some quantitative insight into the factors that affect the failure probability of embankments and may prove useful in the decision-making process during the design. However, this paper is concerned with illustrating how these results can be used during the acceptance stage of the embankment construction.

Because only a limited number of samples are taken during the inspection process, the mean E and the variance are not known with certainty. The uncertainty in E resulting from limited sampling can be approximated by the student t distribution.

$$f(z) = \frac{1}{\sqrt{\pi(n-1)}} \frac{\Gamma\left(\frac{n}{2}\right)}{\Gamma\left(\frac{n-1}{2}\right)} \left(1 + \frac{z^2}{n-1}\right)^{-n/2} \qquad (2)$$

where $z = \overline{E}^* - \overline{E}/\sqrt{S_E^2/[n(n-1)]}$; $\overline{E}$ is the actual mean of the earth mass; S_E^2 and $\overline{E}^*$ are the calculated variance and mean of E respectively, based on the n samples taken; and

$\Gamma(\cdot)$ is the gamma function. Combining Eqs. 1 and 2 and performing some mathematical manipulation give the failure probability with limited knowledge.

$$P_f = P(\delta > \bar{\delta} F_s) = \int_0^{\infty} P(\delta > \bar{\delta} F_s \mid E)\, f(\bar{E})\, d\bar{E}$$

$$= \int_{-\infty}^{\infty} \int_{-\infty}^{-\frac{\bar{k}}{\sigma_k}\left(F_s - \frac{\beta}{\eta}\right)} \frac{1}{\pi \alpha \beta} \sqrt{\frac{n}{2}}\, \frac{\Gamma\left(\frac{n}{2}\right)}{\Gamma\left(\frac{n-1}{2}\right)} \left(e^{-x^2/2}\right) \left[1 + n\left(\frac{1-\eta}{\alpha\beta}\right)^2\right]^{-n/2} dx\,d\eta \qquad (3)$$

in which $\alpha = S_E/\bar{E}_d$ and $\beta = \bar{E}_d/\bar{E}^*$, where $\bar{E}_d$ is the design mean of E, and $\eta = 1 - [\alpha\beta/\sqrt{n(n-1)}]\ z = \bar{E}/\bar{E}^*$.

In the limit $\{(-\bar{k}/\sigma_k)\ [F_s - (\beta/\eta)]\}$ of Eq. 3, values of η are restricted to being positive inasmuch as E is positive. Mathematically the student t distribution accounts for both positive and negative values of η. However, for the range in the α and β values of practical interest, the probability density function describing η is for all practical purposes generally 0 on the negative η axis if n is larger than 5. If n is smaller than 5, Eq. 2 must be replaced by a probability density function appropriate for describing the uncertainty in the mean of a positive random variable, and appropriate changes would be required in subsequent equations using Eq. 2.

The parameter $\bar{k}/\sigma_k$, which is used in Eq. 3, is a function of the C_{VE}. Both the standard deviation of E and C_{VE} are uncertain. Although it is possible, with additional mathematical effort, to include the uncertainty of C_{VE} in the analysis, the additional effort is deemed unwarranted at this stage. For given soil conditions and normal product control measures, a reasonable estimate for the coefficient of variation of the soil property can be made even with a limited number of samples. If a reasonable estimate of C_{VE} can be made, the ratio $\bar{k}/\sigma_k$ can be determined for a given slope angle and embankment geometry as suggested by Kraft and Yeung (7).

A typical result obtained from Eq. 3 is shown in Figure 6. As the reciprocal of β increases, the failure probability decreases. The magnitude of the decrease in P_f is influenced by C_{VE}, the slope angle and geometry, Poisson's ratio, α, F_s, and the number of samples taken to determine β. The larger the number of samples is, the greater the confidence will be that the actual mean E is equal to the measured mean $\bar{E}^*$; hence, for a given β the failure probability decreases as n increases.

Treating $\bar{E}$ as a random variable accounts for the possibility that the actual mean may be greater than the design $\bar{E}_d$ and, thus, accounts for the contractor's risk. At the same time, the possibility that the actual mean is less than the design mean is also accounted for in probabilistic terms; thus, the owner's risk is accounted for. If the maximum permissible failure probability can be established, the results obtained with Eq. 3 can be represented in a graphical or tabular form readily usable for field execution. Before that representation is illustrated, however, a few comments on the maximum permissible P_f are in order.

DESIGN CRITERION

Because the acceptance specifications should reflect the design philosophies and design considerations in some way, these comments are made on the design criterion. The optimum selection of the failure probability may be based on minimizing the total expected cost of the embankment. The total expected cost consists of the construction cost (usual maintenance costs are assumed to be included) and the expected risk cost. For a given embankment geometry and soil, the construction cost usually increases with a decrease in the failure probability. The risk cost (or failure cost) increases with an increase in the failure probability. Adding the construction cost and risk cost

Figure 1. Simulation of statistically heterogeneous embankment by finite elements.

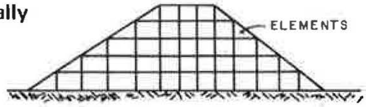

Figure 2. Mean slope deformations of a statistically heterogeneous embankment.

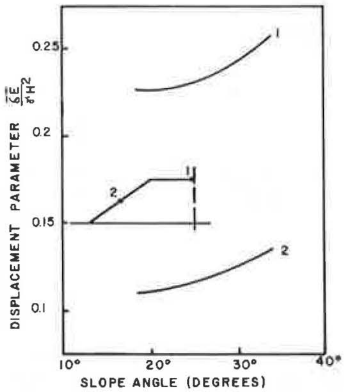

Figure 3. Concept of safety factor.

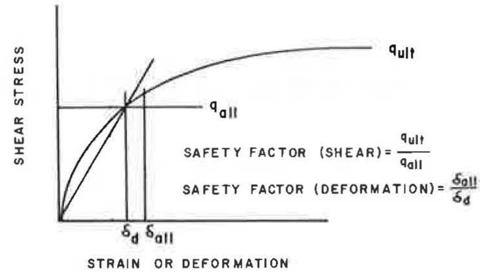

Figure 4. Embankment geometry.

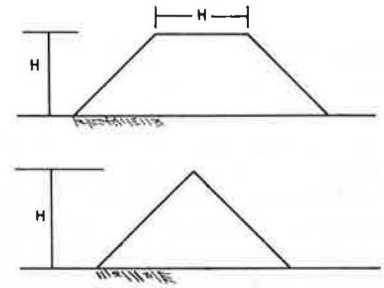

Figure 5. Influence of safety factor on failure probability knowing the mean soil stiffness.

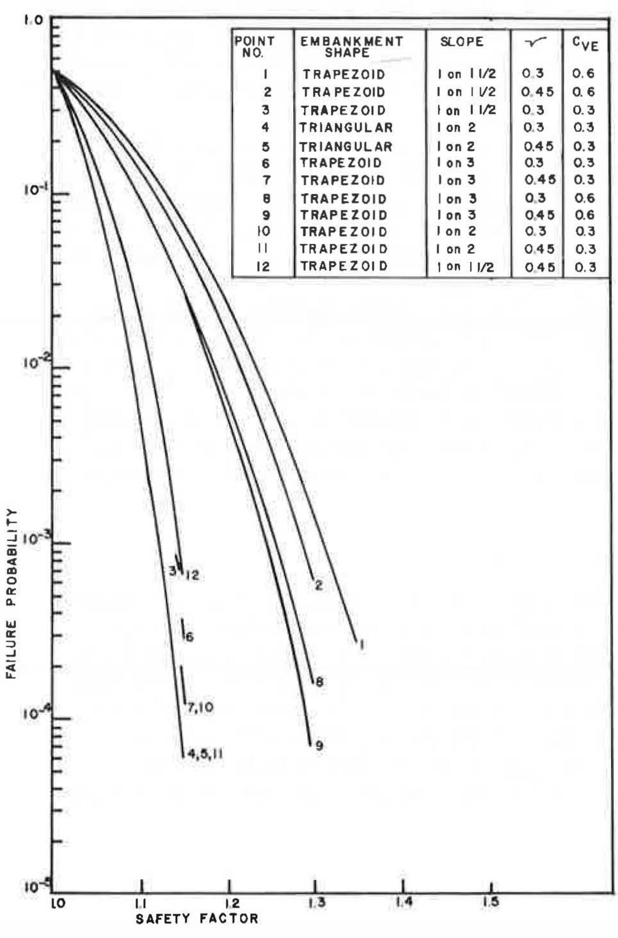

POINT NO.	EMBANKMENT SHAPE	SLOPE	ν	C_{VE}
1	TRAPEZOID	1 on 1 1/2	0.3	0.6
2	TRAPEZOID	1 on 1 1/2	0.45	0.6
3	TRAPEZOID	1 on 1 1/2	0.3	0.3
4	TRIANGULAR	1 on 2	0.3	0.3
5	TRIANGULAR	1 on 2	0.45	0.3
6	TRAPEZOID	1 on 3	0.3	0.3
7	TRAPEZOID	1 on 3	0.45	0.3
8	TRAPEZOID	1 on 3	0.3	0.6
9	TRAPEZOID	1 on 3	0.45	0.6
10	TRAPEZOID	1 on 2	0.3	0.3
11	TRAPEZOID	1 on 2	0.45	0.3
12	TRAPEZOID	1 on 1 1/2	0.45	0.3

Figure 6. Influence of sampling results on failure probability.

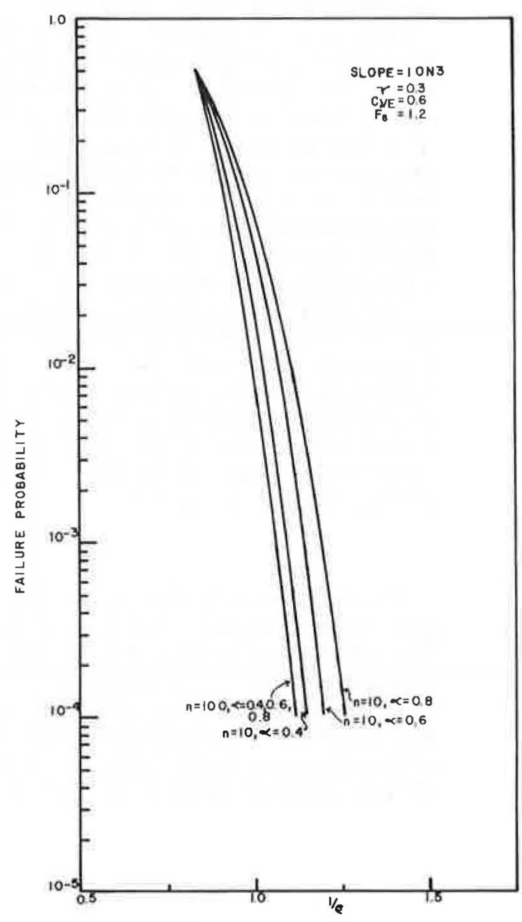

results in the total expected cost as shown in Figure 7. The failure probability corresponding to the minimum cost represents the optimum for the stated conditions. Provided such cost functions can be established, the maximum permissible failure probability, denoted as P_{f_m}, can be determined with this approach.

An alternative, which is more straightforward but less quantitative, for establishing P_{f_m} is to arbitrarily select P_f as some small number. The smallness of the number should be such that for all practical purposes the failure probability is 0. This alternative is used here, and 2 values of the maximum permissible P_f (namely, 10^{-2} and 10^{-4}) are used for purposes of comparison.

PRODUCT CONTROL CHARTS

For a given slope geometry, Poisson's ratio, C_{VE}, and α, the value of $1/\beta$ corresponding to P_{f_m} can be determined for different values of n from graphs such as those shown in Figure 6. These limiting or critical values of $1/\beta$ will be denoted as $1/\beta_c$. Only values of $1/\beta$ greater than $1/\beta_c$ constitute an acceptable unit of work. Values of $(1/\beta_c)$ plotted against the number of samples for a variety of conditions are shown in Figure 8. The results show that a much larger value of $1/\beta_c$ is required for values of n on the order of 5 than for values of n on the order of 10 to 20. Values of $1/\beta_c$ larger than 1 correspond to measured values of the mean $\overline{E}^*$ being greater than the design mean $\overline{E}_d$. Because of the advent of more rapid field-measuring devices, the cost and time of taking 10 to 20 samples in a given section are not at all prohibitive. The attainment of more samples allows for a reduction in the required $1/\beta_c$, which the contractor would probably welcome, and at the same time does not increase the risk, as defined by the probabilities, to the owner or engineer.

On the basis of test results from n samples, a decision must be made to accept or reject a unit of work as currently compacted. A unit of work may conveniently be taken as the volume compacted during a specified time period such as 1 day. Methods for defining units and for randomly selecting subunits within the unit for testing are available in the literature (12, 16) and will not be repeated here. Because the results of the model presented in this paper are based on a relatively homogeneous earth mass, the acceptance or rejection of each unit of compacted soil must be made on the basis of test results solely from the respective unit. Thus, a relatively uniform completed project is ensured. If the cross section consists of zones of different materials and if the zoning conditions are known ahead of time, it would be feasible to develop the corresponding control charts.

The results shown in Figure 8 demonstrate that, as the design safety factor F_s increases, the value of $1/\beta_c$ decreases. In other words, the greater the conservatism in the original design is, the more relaxed the acceptance requirements can be. The presented results provide a quantitative measure of those factors.

As the maximum permissible failure probability decreases, the value of $1/\beta_c$ increases. The results shown only include a comparison of $P_{f_m} = 10^{-2}$ and $P_{f_m} = 10^{-4}$. For practical purposes, a failure probability of 10^{-4} or smaller may be considered as 0.

The coefficient of variation of a compacted soil property is dependent on many factors including the soil itself. For soils with a greater natural heterogeneity, the coefficient of variation is likely to be larger than for more uniform soils even with strict product control (12). A comparison of Figures 8e and 8f demonstrates that a larger $1/\beta_c$ is required for the more heterogeneous soil. As an approximation, $1/\beta_c$ corresponding to a C_{VE2} can be obtained from

$$\left(\frac{1}{\beta_c}\right)_2 \sim \frac{C_{VE2}}{C_{VE1}}\left[\left(\frac{1}{\beta_c}\right)_1 - 1\right] + 1.0 \tag{4}$$

where $(1/\beta_c)_1$ corresponds to the condition for C_{VE1}.

Although most of the above results are intuitively obvious, they do provide a quantitative measure. It is illustrated in the following section how these results can be applied in terms of moisture and density.

Figure 7. Optimization concept.

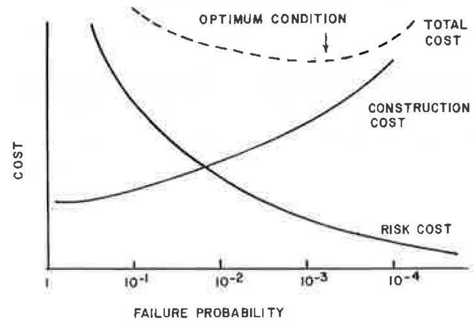

Figure 8. Acceptance requirements.

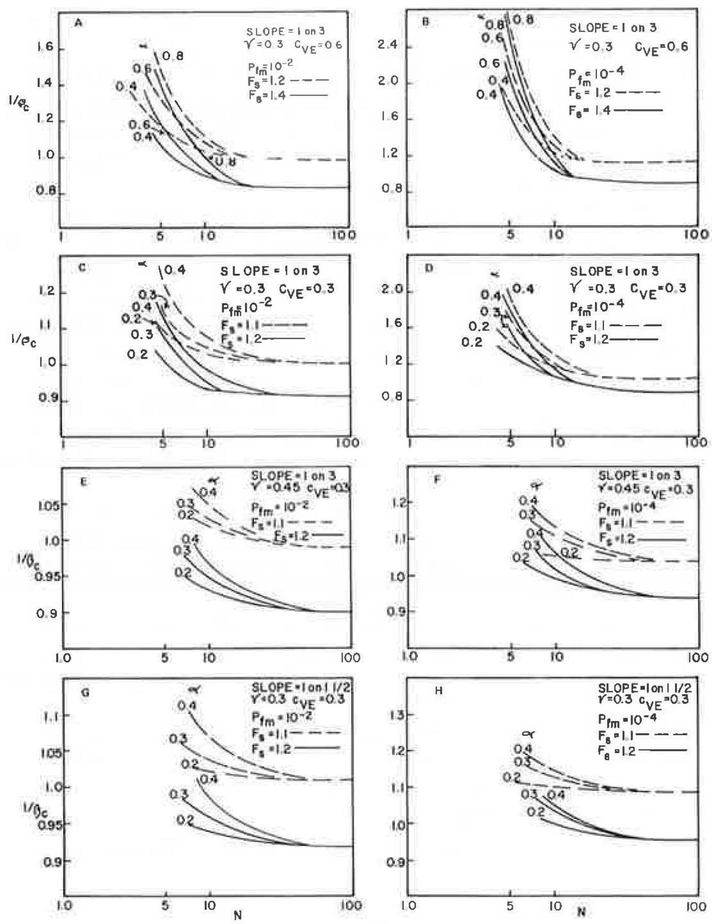

MOISTURE AND DENSITY CONTROL

Strength, stiffness, swelling potential, and permeability of the soil govern the performance of an earth mass and for a given soil and compaction technique can be related to the moisture and density of the soil. Because field control is based on moisture and density, the following arguments are presented to illustrate the application of the results found in this study.

For a particular soil, relations can be established between dry density and strength and between water content and strength. In this example, the data obtained by Seed and Chan (10) for a plastic clay are used. The strength relation can be approximated by the linear equation

$$s_u = a\,\gamma_d + bw + c \tag{5}$$

where s_u is the undrained shear strength, γ_d is the dry density, and w is the water content expressed as a percent. The constants for the plastic clay are equal to 11,570 cm, -0.488 kg/cm^2, and -6.15 kg/cm^2.

Inasmuch as the above data pertain to laboratory-compacted specimens, it may be questioned whether Eq. 5 can be applied to field-compacted soils. However, Seed and Chan have shown that different laboratory-compaction procedures lead to about the same ultimate strength for a given water content and dry density. Agreement between the strengths of laboratory- and field-compacted soils has been reported by Holtz and Ellis (6). Hence, in the subsequent analysis, it is assumed that there is no difference between the shear strength of laboratory-compacted and field-compacted specimens.

It must be noted that the constants a, b, and c may be different for different soils. Also the linear approximation of the strength may not be applicable for all soils. However, there are insufficient data to establish the nature of such variations. Hence, this analysis is restricted to soils similar to those studied by Seed and Chan.

A further assumption is required to relate the elastic modulus E to the undrained strength. For purpose of demonstration, the elastic modulus is taken to be proportional to the undrained strength. Hence, the β value in terms of moisture and density is

$$\beta = \frac{a\,\overline{\gamma}_d + b\overline{w}_d + c}{a\,\overline{\gamma}_d^* + b\overline{w}^* + c} \tag{6}$$

where $\overline{\gamma}_d$ and $\overline{w}_d$ are the mean values used in the design, and $\overline{\gamma}_d^*$ and $\overline{w}^*$ are the measured means (dry density and water content). Equation 6 is based on γ_d and w being statistically independent. The validity of that assumption is discussed further in later paragraphs. If, for an acceptable unit of work, β must be less than β_c, then

$$\overline{\gamma}_d^* + \frac{b}{a}\overline{w}^* + \frac{c}{a} - \frac{\overline{\gamma}_d + \frac{b}{a}\,\overline{w}_d + \frac{c}{a}}{\beta_c} \geq 0 \tag{7}$$

For a given job, the parameters a, b, c, $\overline{\gamma}_d$, $\overline{w}_d$, and β_c are known. Using the equality sign, Eq. 7 is shown in Figure 9 in terms of different β_c values, which can be determined from Figure 8. If the measured values $\overline{\gamma}_d^*$ and $\overline{w}^*$ plot above the line for the respective β_c value, the unit of work is considered acceptable. The results shown in Figures 8 and 9 can be combined into a single graph; however, there is no apparent advantage in consolidating them. Figure 8 can be used to establish β_c, and then Figure 9 can be used with the corresponding value of β_c.

The coefficients of variation for moisture content and dry density are typically on the order of 0.1 and 0.05 respectively, as evidenced by published data (2, 14, 15). Most of the moisture and density conditions will be between ±2 standard deviations from the mean. If the mean is equal to the design condition, the moisture and density condition should fall within the shaded region shown in Figure 9 for the design conditions shown.

It is well established that the control of the moisture content is crucial for obtaining the proper density. Hence, some dependence between moisture and density is to be expected. However, for a moisture content range of 2 to 3 percent, there is evidence that moisture and density may be assumed to be independent, at least for some soils. Torrey (14) presents results from 5 materials in the construction of the Littleville Dam on Westfield River in Massachusetts. His results illustrate that the assumption of independence may serve as a good first approximation. With that assumption, it can then be stated that the probability that a unit of work will satisfy the specification increases as the area of the shaded region below the respective $1/\beta_c$ line (Fig. 9) decreases. One may also observe that the probability of satisfying the specification is less if the measured mean moisture content is on the wet side than if it is on the dry side for the given soil.

Obviously, consideration must be given to several factors such as swelling potential, strength, stiffness, and permeability in establishing the testing procedure for determining the relation between soil stiffness and moisture-density. For the concepts of this paper to be applied, the attainment of the soil stiffness as related by moisture and density must incorporate those considerations. If the relation is nonlinear, appropriate modifications in the formulation must be made. For example, it has been reported (18) that for soils compacted on the dry side of optimum moisture the strength increases with the square of the dry density.

$$s_u = a + b\gamma_d^2 \tag{8}$$

Again, if the elastic modulus is taken to be proportional to the undrained strength, the β value is

$$\beta = \frac{a + b\overline{\gamma}_d^2}{[a + b(\overline{\gamma}_d^*)^2 + S_\gamma^2]} \tag{9}$$

where S_γ^2 is the measured variance of the dry density. The mean of the square of a random variable is not the same as the mean squared. The quantity in the brackets of the denominator of Eq. 9 is the mean of the square of γ_d. For a silty clay, the constants a and b were found to be -11.25×10^6 kg/cm^2 and 3.95×10^6 cm^4/kg, based on a density ranging between 1.68 and 1.76×10^{-3} kg/cm^3.

For other relations among strength, moisture, and density, the appropriate modifications can be made. The following illustration is limited, however, to conditions representative of Eq. 6.

ILLUSTRATION

The design conditions shown in Figure 9 are applied to a 1:3 embankment with a design safety factor of 1.2 and a maximum permissible failure probability of 10^{-4}. The values of $1/\beta_c$ as influenced by the sample size n are given in Table 1; a $C_{VE} = 0.3$ (Fig. 8d) is used. If only 5 samples are taken and if the shaded area shown in Figure 9 is representative of the field condition, the probability of accepting the work is much smaller than if 10 or more samples are obtained. On the other hand, if the field moisture conditions are on the wet side of the design values, resulting in the shaded area being shifted to the right and possibly downward, the probability of accepting the work will be small regardless of the number of samples taken.

As a means for illustrating the use of the results of the paper, suppose that a mean moisture content and dry density of 20 percent and 1.8×10^{-3} kg/cm^3 and an α value of 0.25 have been obtained from 10 samples. For the previously stated condition, should the unit of work on which the data are based be accepted? From Figure 8d, a value of $1/\beta_c$ equal to 1.08 is estimated. Because the point (20 and 1.8×10^{-3}) plots above the line corresponding to $1/\beta_c = 1.08$, the unit would be accepted.

The pertinent charts or graphs can easily be used by field personnel. The additional effort required is not prohibitive, and the use of charts reduces the risk of computational errors.

Most statistical specifications for compaction control give consideration only to the uncertainties resulting from limited sampling. The model developed here considers the influence of both spatial uncertainties and sampling uncertainties; therefore, it is of interest to compare these results with those obtained when only limited sampling is considered. If the design is based on the mean soil property governing the performance

Figure 9. Compaction requirements in terms of moisture and density.

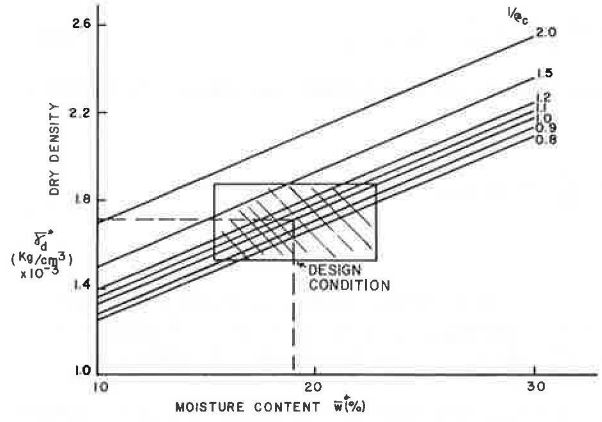

Table 1. Values of $1/\beta_c$.

n	α = 0.2	α = 0.3	α = 0.4
5	1.28	1.56	1.80
10	1.04	1.08	1.16
100	0.92	0.92	0.92

Figure 10. Acceptance requirements neglecting spatial variations.

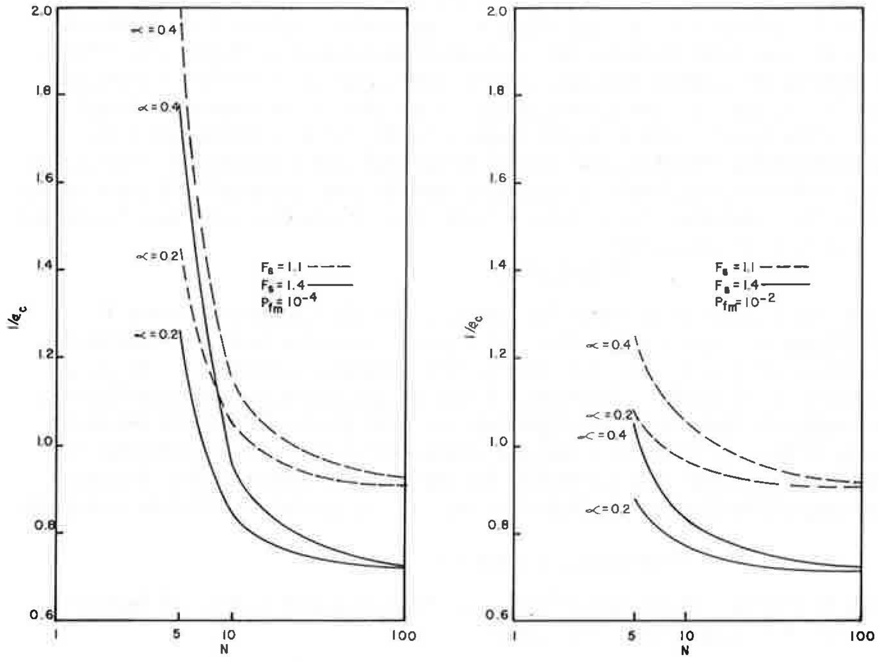

Figure 11. Effect of not including the influence of spatial variations in acceptance requirements.

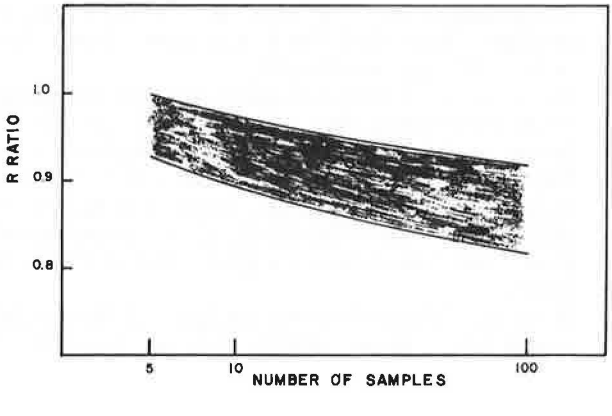

of the earth mass, the failure probability is

$$P_f = P[\delta > F_s\bar{\delta}] = P[\bar{E} < \bar{E}_d/F_s] \tag{10}$$

The student t distribution is used to account for the uncertainties contributed to limited sampling, and the failure probability is

$$P_f = 1 - \int_{-\infty}^{\frac{1-\beta/F_s}{\beta}\sqrt{n(n-1)}} f(z)\,dz \tag{11}$$

Equation 11 can be used to generate curves similar to those shown in Figure 8. The values of $1/\beta_c$, if the influence of spatial uncertainties is neglected, are not influenced by the angle of the slope, the geometry of the slope, or the magnitude of Poisson's ratio.

The importance of neglecting those factors can be estimated by comparing the results shown in Figure 10 with those shown in Figure 8. The ratio R of the $1/\beta_c$ requirement neglecting the spatial uncertainty (Eq. 11) to the $1/\beta_c$ requirement considering both spatial and sampling uncertainties (Eq. 3) will be used for purposes of comparison. An R value greater than 1 indicates that neglecting the spatial uncertainty is conservative. A range of the R values obtained for slope conditions shown in Figure 8 is shown in Figure 11. Neglecting the spatial variation of the soil properties in the acceptance criterion, as shown in Figure 11, can result in the acceptance requirements being too low. The influence of the spatial variation increases as the number of samples increases, if both uncertainties (spatial and limited sampling) are considered. For small values of n, the uncertainty due to limited sampling has the predominant influence on the acceptance requirements; whereas, for larger values of n, the uncertainty due to spatial variation has the predominant influence.

SUMMARY

The results of the study provide quantitative insight into the factors affecting the acceptance specifications of earth compaction. The results can be used for establishing acceptance specification guidelines and are readily adapted to field use. Several simplifying assumptions were made. However, it is the opinion of the authors that the results clearly demonstrate that, if the acceptance is based on the measured mean as compared to a design value, 10 or more samples should be required for each unit of work. Because random sampling is a necessity for the use of these results, the size of each unit of work should be limited so that it is convenient to obtain random samples.

ACKNOWLEDGMENT

The authors wish to express their appreciation to the Computer Center of Auburn University for assistance in conducting this study.

REFERENCES

1. D'Appolonia, D. J., Poulos, H. G., and Ladd, C. C. Initial Settlement of Structures on Clay. Jour. Soil Mech. and Found. Div., Proc., ASCE, Vol. 97, No. SM10, Paper 8438, 1971, pp. 1359-1377.
2. Davis, F. J. Quality Control of Earth Embankments. Proc., 3rd Int. Conf. on Soil Mech. and Found. Eng., Vol. 1, 1953, pp. 218-224.
3. Davis, F. J. Summary of Bureau Experiences in Statistical Control of Earth Dams Embankment Construction. Proc., Nat. Conf. on Stat. Qual. Control Methodol. in Highw. and Airfield Const., Univ. of Virginia, 1966.
4. Gould, J. P., and Dunnicliff, C. J. Accuracy of Field Deformation Measurements. Proc., 4th Pan-American Conf. on Soil Mech. and Found. Eng., Vol. 1, 1971, pp. 313-366.
5. Hoeg, K. Finite Element Analysis of Strain-Softening Clay. Jour. Soil Mech. and Found. Div., Proc., ASCE, Vol. 98, No. SM1, Paper 8650, 1972, pp. 43-58.

6. Holtz, W. G., and Ellis, W. Comparison of the Shear Strengths of Laboratory and Field-Compacted Soils. In Laboratory Shear Testing of Soils, ASTM, STP 361, 1963, pp. 471-480.
7. Kraft, L. M., Jr., and Yeung, J. Simulating Deformations of Statistically Heterogeneous Earth Structures. Submitted for publication.
8. Langfelder, L. J., and Nivargikar, V. R. Some Factors Influencing Shear Strength and Compressibility of Compacted Soils. Highway Research Record 177, 1967, pp. 4-21.
9. Lumb, P. Some Factors and the Probability Distribution of Soil Strength. Canadian Geotechnical Jour., Vol. 7, No. 3, 1970, pp. 225-242.
10. Seed, H. B., and Chan, C. K. Structure and Strength Characteristics of Compacted Clays. Trans., ASCE, Vol. 126, 1961.
11. Seed, H. B., Mitchell, J. K., and Chan, C. K. The Strength of Compacted Cohesive Soils. Proc., Res. Conf. on Shear Strength of Cohesive Soils, Boulder, Colo., 1960, pp. 887-964.
12. Sherman, G. B., Watkins, R. D., and Prysock, R. H. A Statistical Analysis of Embankment Compaction. Highway Research Record 177, 1967, pp. 157-185.
13. Singh, A., and Lee, K. L. Variability in Soil Parameters. Proc., Symp. of Eng. Geol. and Soils Eng., Boise, April 1970, pp. 159-185.
14. Torrey, V. H., III. Analysis of Field Compaction Data: Report 2—Littleville Dam, Westfield River, Massachusetts. U. S. Army Engineer Waterways Experiment Station, Vicksburg, Miss., Misc. Paper 5070-B, 1970.
15. Turnbull, W. J., Compton, J. R., and Ahlvin, R. G. Quality Control of Compacted Earthwork. Jour. Soil Mech. and Found. Div., Proc., ASCE, Vol. 92, SM1, Paper 4623, 1966, pp. 93-103.
16. Weber, W. G., Jr., and Smith, T. Practical Applications of the Area Concept to Compaction Control Using Nuclear Gages. Highway Research Record 177, 1967, pp. 144-156.
17. Wu, T. H., and Kraft, L. M., Jr. Safety Analysis of Slopes. Jour. Soil Mech. and Found. Div., Proc., ASCE, Vol. 96, No. SM2, Paper 7174, 1970, pp. 609-630.
18. Yoder, E. J. Selection of Soil Strength Values for Design of Flexible Pavements. Univ. of Western Australia, Res. Rept., May 1968.

APPLICATION OF STRAIN MEASUREMENTS TO SOIL COMPACTION EVALUATION

Ernest T. Selig, State University of New York at Buffalo

The purpose of this study was to investigate the use of soil strain measurements for observing compaction of earth materials in the field. The sensors consisted of disk-shaped coils embedded in the material; the distance between adjacent pairs was determined by inductance coupling. Experiments were conducted on portions of an Interstate highway in New York and on a special test section at the Waterways Experiment Station in Vicksburg, Mississippi. Techniques for sensor installation were developed, possible field applications were demonstrated, and advantages and limitations of the concept for compaction evaluation were determined. The instrumentation system performed satisfactorily in the field construction environment. The sensors survived compaction in crushed slag and gravelly backfill. The measurement of vertical and horizontal strains permitted calculation of percentage of density change. Resolution was about 0.1 percent strain under normal conditions. A recorder detected much smaller changes. Strain measurements were particularly useful for evaluating variation of compaction with depth, compaction changes with each roller pass, secondary compaction as additional layers were added, variability of end results, and difference in capability between compactors.

•METHODS of evaluating field compaction of highway materials have been limited almost entirely to surface density measurements. The devices used include a sand cone, rubber balloon, or nuclear detector, which, in some materials, such as rockfill, lightweight aggregate, and variable till, may be unsatisfactory. In addition, the methods are impractical for use in investigating important factors such as the variation of compaction with depth, the benefit of each successive roller pass, the change that occurs in lower layers during compaction of the surface lift, the relative effectiveness of alternative compactors, and the long-term volume changes in compacted fills associated with consolidation and with moisture and temperature variations. Because compaction is a process of densifying the material by decreasing its volume, volumetric strain is a direct quantitative measure of the amount of compaction. Therefore, a strain sensor embedded in the material is a conceptually feasible way to investigate compaction factors.

The objective of the study reported in this paper was to investigate the feasibility of using newly developed instrumentation (1) and, in the process, to establish techniques for its application in the field. Field experiments were conducted during the summer of 1970 in connection with construction of a portion of Interstate highway in the vicinity of Olean and Jamestown, New York. Those experiments were followed by special compaction tests in January 1971 at the Waterways Experiment Station in Vicksburg, Mississippi. The latter tests provided the opportunity to complete the assessment of the techniques through controlled conditions that were not present during the summer construction operations. A detailed description of this research is given in an earlier report (2).

INSTRUMENTATION SYSTEM

The strain gauge system consists of a pair of embedded sensors and an external instrument package connected by electrical cables. The sensors, each of which is a disk-shaped coil, are placed in the soil in either coaxial alignment (Fig. 1) or coplanar alignment (Fig. 2). They are separated a distance over which the strain is to be averaged. A matrix combining the coaxial and coplanar configurations may also be used (Fig. 3). The coil diameter can be selected to fit the job requirement. To date, diameters ranging from 1 to 14 in. have been tested. In this study, only the 4-in. size was used because sensor spacings in the range of 6 to 12 in. were desired. Durability and low cost were considerations involved in sensor design.

The principle of operation is based on mutual inductance between the coil sensors. A 20-kHz frequency current is established in one of the coils and creates a magnetic field encompassing the second coil in the pair. That induces a current in the second coil, the magnitude of which is directly related to the separation of the sensors.

An important feature of the system is that the sensors are free-floating in the soil to provide minimal interference with the soil movement. The system is electrically designed to operate at any sensor spacing between 1 and 4 times the nominal sensor diameter. The effects of rotational or transverse movements, which cause misalignment, are normally of second order compared to the primary effect of spacing change. The effect of soil moisture and temperature change is negligible, and rarely does soil composition have to be considered. Finally, the effect of different cable lengths is small and can easily be accounted for during calibration. Verification of these characteristics is given in earlier reports (1, 3, 4).

The bridge balance is accomplished on the external instrument package by means of phase and amplitude controls; a meter is used to indicate null. The amplitude digital dial reading corresponds to the sensor spacing. Changes in spacing may be determined by renulling and noting the changes in the amplitude reading. They may also be determined by meter deflection from zero or by voltage output on a recorder connected to the rear panel. When these latter methods are selected, the calibration control is used to adjust the output sensitivity so that it corresponds to a desired amount of strain. The instrument is battery-operated and completely portable, which is a convenience especially desirable in the field.

The method of system calibration is conceptually simple. The sensors are aligned in either the coaxial or coplanar configuration, and amplitude readings are obtained for appropriate sensor spacings. Calibration curves are then drawn relating spacing to amplitude and strain to change in amplitude. A fixture like that shown in Figure 1 for positioning the sensors at known coaxial spacings simplifies and expedites the calibration process.

RESULTS OF FIELD TESTS

The field installation plan depends on the particular application for which the sensors are being used. The procedures are different for compaction with a sheepsfoot roller and for compaction with a smooth-drum roller. The requirements are different for granular backfill and for cohesive embankment material. Finally, a distinction must be made between the large strains during initial compaction and the smaller long-term changes. The experiments conducted in this study were directed toward one or more of these situations in order to establish techniques and assess the suitability of the instrumentation. Examples of the results are described in this paper. Detailed descriptions of the tests and sensor-installation procedures are given in another report (2).

Some of the strain data were used to estimate density changes from compaction. In doing so, the relation used was that the percentage of change in density from the initial state equals the sum of the vertical, longitudinal, and transverse strains, expressed as a percent. If, for example, the horizontal strains (longitudinal and transverse) are small compared to the vertical strain, then the percentage of density change will approximately equal the percentage of vertical strain.

Embankment Compaction

The first example involves a matrix of 9 sensors installed in a rocky till embankment material compacted in 8-in. lifts by a sheepsfoot roller. The sensors were placed 3 each in a coplanar configuration (Figs. 2 and 3) at the top of 3 successive lifts after compaction. Additional lifts were then deposited and compacted. The sensors provided measurement of horizontal strains during primary compaction (compaction of the soil when it is the surface layer), both parallel and perpendicular to the direction of roller travel, and vertical strains through the lifts during secondary compaction (subsequent compaction of a lift during placement and rolling of superimposed lifts).

The results suggested that satisfactory sensor performance can be obtained during secondary strain observation in a variable embankment material, even with a sheepsfoot roller, when the sensors are placed at the top of each compacted lift after the loose surface material is removed. Because the lifts were too thin, no information was obtained in this experiment on the vertical strains during primary compaction. The magnitude and sign of the horizontal strains were quite variable (Fig. 4). Large horizontal strains occurred only during the first few roller passes of primary compaction, if at all; subsequent changes were small. The 3 vertical sets of sensors in each lift showed the same trends for strain although the magnitude varied among them (Fig. 5). In every case, the significant strains were compressive. The observed differences are believed to be a result of the variability of the fill material. Compressive strains were observed to occur in the instrumented layers during secondary compaction of 3 subsequent lifts; thereafter changes were small. The equivalent density change associated with the secondary strains appeared to be as much as 6 lb/ft^3.

Granular Backfill Compaction

In the second example, 21 sensors were installed in coplanar groups of 3 between successive lifts of granular material being placed adjacent to sheet piling (Figs. 6 and 7). The material was deposited by truck, spread in 6-in. layers with a bulldozer, and compacted by self-propelled, smooth-drum vibratory roller. The sensors measured horizontal strains, both parallel and perpendicular to the direction of roller travel, and vertical strains through the lifts. Some 6-in. lifts were not compacted until the next lift was placed, giving the effect of a 12-in. lift spread in two 6-in. sections. This procedure provided information on the strains during primary compaction. In the remaining cases, the strains were recorded only for secondary compaction.

The strain sensors were found to be suitable for application to coarse granular material. The use of a smooth-drum roller permitted simple and accurate sensor placement on the compacted lift surface.

After primary compaction of 6-in. lifts with roller passes on the order of 6 to 8, secondary density changes still occurred during compaction of the next 2 to 6 lifts or 1 to 3 ft of fill (Fig. 8). Increases of as much as 6.5 lb/ft^3 were estimated from the data. Horizontal strains tended to be compressive in the direction of roller travel and extensional in the transverse direction. Usually, these strains did not change significantly after the lift directly on top of the sensors had been compacted. The vertical strains were observed to vary by 50 percent or more within a 1-ft diameter circle. These appear to be real differences resulting from variability of the material, particularly the size and number of the large particles, in the area of the sensors.

Stacking Evaluation

In the third example, a group of 16 sensors and 2 settlement platforms were installed in a till embankment material delivered by truck and spread with a bulldozer (Fig. 9). Compaction was specified in 12-in. lifts with either a sheepsfoot roller or a self-propelled, smooth-drum vibratory roller. The settlement device was of the water overflow type and was connected by plastic tubes to a readout post. The sensors were placed on top of each successive lift after compaction. Thus, only secondary strains were measured. The settlement platforms provided a means of correcting initial rod readings for subsequent sensor settlement in order to compare them with the embankment movements indicated from the strain gauge readings. The sensors were located in 2 separate vertical stacks to provide a replicate measurement for evaluating strains.

As a result of the wide variations in construction procedures, the final strains were quite different among the group of lifts (Fig. 10). However, the strains measured at

Figure 1. Sensors in coaxial configuration for rapid calibration.

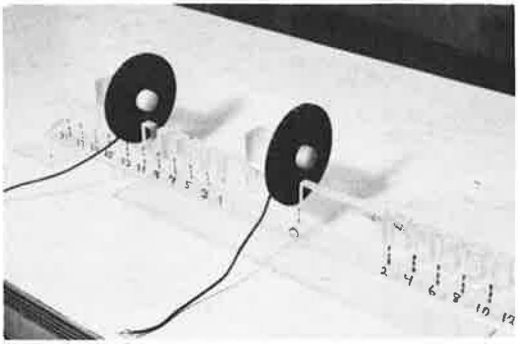

Figure 2. Sensors in coplanar configuration for horizontal strains in embankment.

Figure 3. Sensor layout for embankment test using matrix to obtain vertical and horizontal strains.

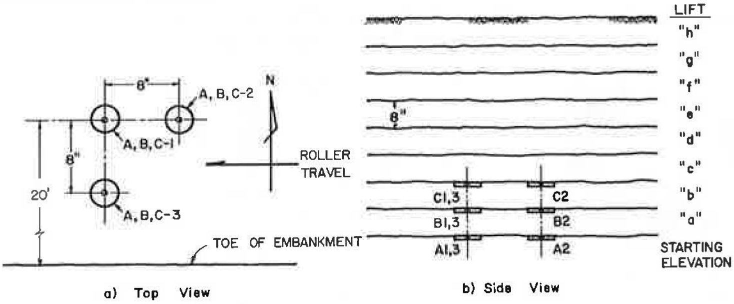

Figure 4. Horizontal strains for embankment compaction.

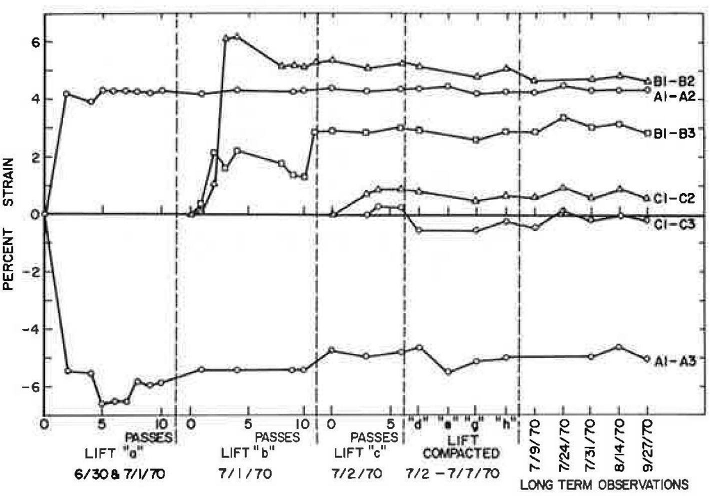

Figure 5. Vertical strains for embankment compaction.

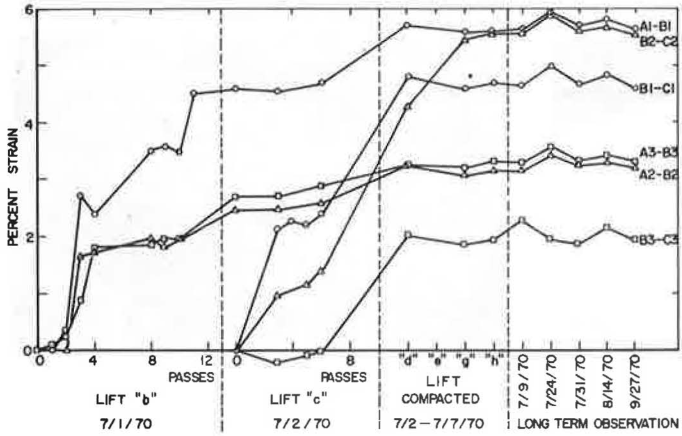

Figure 6. Covered sensors and cables before deposit of loose lift.

Figure 7. Sensor configuration in granular backfill adjacent to sheet piling.

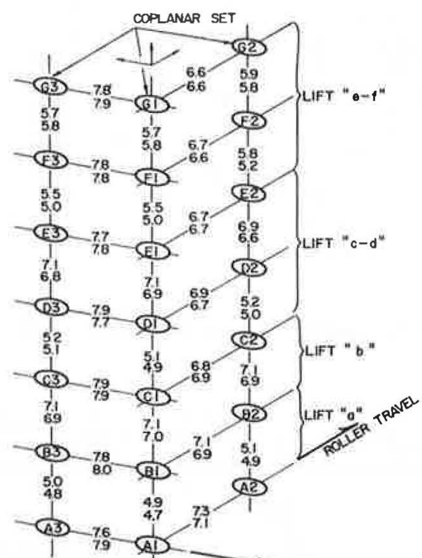

Note: Upper number is spacing after initial placement, and lower one is spacing at end of experiment. Dimensions are in inch.

2 points in the same layer showed general agreement. The differences in replicate measurements may be accounted for by the material variability, although other factors such as placement techniques, also may have contributed to the differences. The largest secondary strain (lift e) occurred because that lift did not receive adequate primary compaction.

The difference in elevation between the lowest and the highest sensors in the fill was measured by summing sensor spacings obtained from the electrical readings. These results were checked with values obtained with a rod and level after adjustments were made for settlement of the lowest sensors. The agreement was within 0.55 to 0.75 percent for 2 instruments, showing that the strain gauge can be used to determine changes over distances greater than the spacing of a single pair of sensors. Agreement between the electrical calculations for each adjacent pair of sensors and the elevation differences was good and within the accuracy of the elevation differences.

Thick-Lift Compaction

The fourth example concerns an experiment performed in a natural gravel fill material in a section of highway embankment. The instrumented test section was formed in this fill by excavating a trench about 4 ft deep and 11 ft wide with a bulldozer. Fourteen sensors were installed in coplanar pairs (Figs. 11 and 12) in the material at successive elevations about 8 in. apart in a single lift having a total height of approximately 56 in. The entire lift was then compacted by a self-propelled, smooth-drum vibratory roller. No compactive effort was applied until all of the sensors had been placed.

The sensors including cables satisfactorily endured the environment imposed by the coarse granular material. The lift thickness determined by summing the coaxial spacings compared well with the rod and level readings.

The sensors were most effective in showing the relative change in compaction with each pass. The strain gauge provided a means of monitoring those changes throughout the entire depth below the surface as rapidly as the roller completes its pass and without disturbing the material (Fig. 13).

The 2 replicate vertical columns of sensors gave similar results (Fig. 14). The differences may be satisfactorily explained by the variation in the granular material properties from point to point in the lift.

The maximum vertical strain occurred at the top of the instrumented section, which was 6 to 14 in. below the surface of the lift (Fig. 14). The minimum vertical strains occurred just below the middepth. Significant strains were produced even at 4 ft below the surface and were believed to have resulted from a saturated moisture condition existing in the bottom portion of the lift and caused by heavy rain prior to compaction. The percentage of density increase caused by compaction as calculated from the vertical and horizontal (transverse) strains was about 18 percent at the top, 7 percent at the midheight, and 10 percent at the bottom of the lift.

Compactor Comparison

The fifth example involved thick-lift compaction of granular material in a trench similar to that in the previous example. In this test, conducted in a covered facility at the Waterways Experiment Station, 2 sets of sensors were used to provide a comparison of operating procedures with a vibratory roller.

Twenty-six sensors were installed in granular material in 2 different stacks, and individual sensors were spaced vertically about 9 in. apart over a total height of approximately 5 ft (Fig. 15). This entire loose lift was then compacted by a self-propelled, smooth-drum vibratory roller. As the roller approached stack A, the vibration frequency was adjusted to give maximum amplitude of drum motion. That condition was held until midway between stacks A and B. At that point, the frequency was changed to 1,800 rpm and held constant until the roller reached the end of the test section.

Nuclear moisture and density readings were made at several depths during lift construction. After compaction, the test section was disassembled carefully to permit checking sensor spacings and to provide the opportunity for final nuclear measurements below the surface.

Figure 8. Vertical strains during backfill compaction.

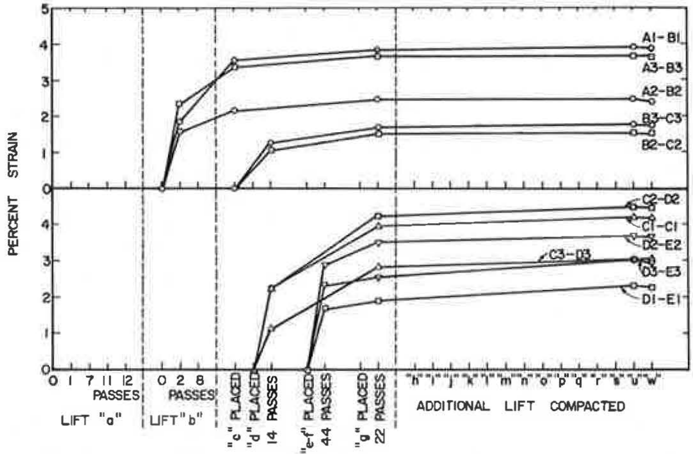

Figure 9. Sensors and remote readout settlement platform in position during checking of level of plane of sensors.

Figure 10. Variation of final strain with depth.

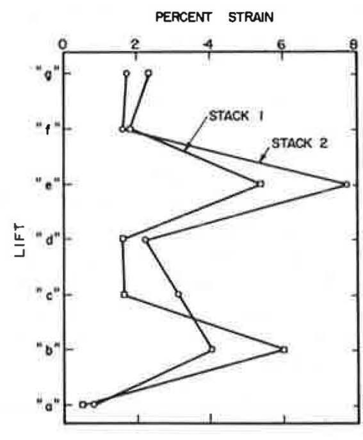

Figure 11. Sensor installation in trench.

Figure 12. Thick-lift compaction sensor array.

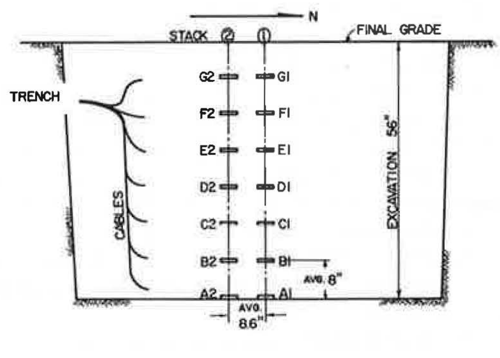

Figure 13. Vertical strain with number of roller passes.

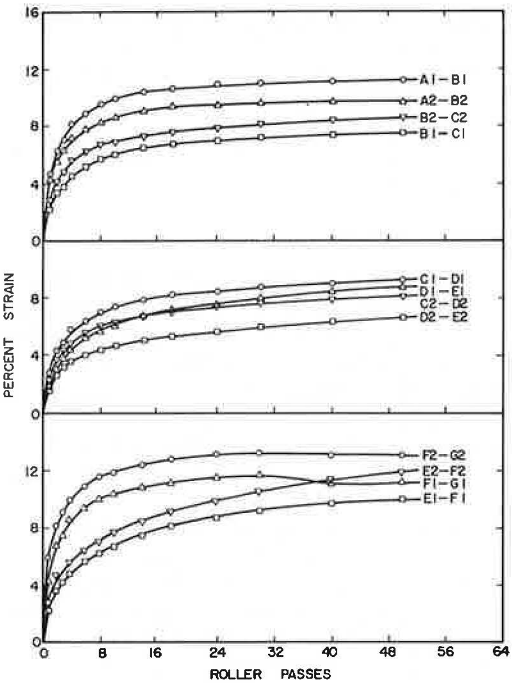

Figure 14. Vertical strain variation with depth after compaction.

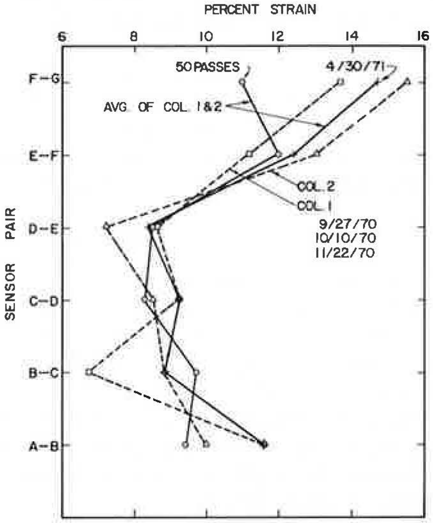

Figure 15. Layout of test section.

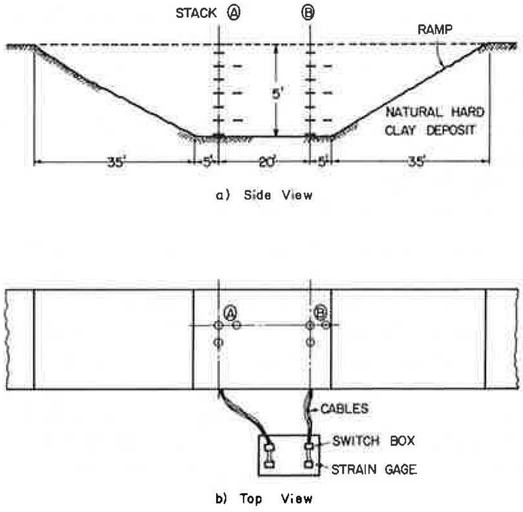

Figure 16. Variation in percentage of density change with depth.

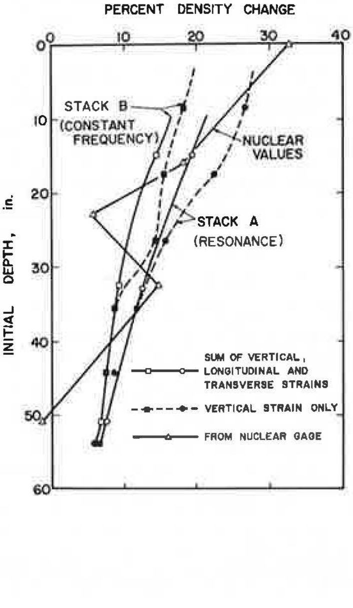

The stack compacted by resonance-seeking procedures experienced significantly greater strains in the top 2.5 ft of the layer than the one compacted by a fixed vibration frequency. However, the differences were very small at the bottom where little compaction was accomplished in either case. Approximate agreement was obtained for percentage of density change computed by the nuclear and strain methods. The discrepancies are attributed to the large variability in density readings, particularly those obtained in the loose soil state (Fig. 16).

The use of switch boxes and 2 instruments made it possible to take the 23 readings after each roller pass in fewer than 5 min. The nuclear instrument was much slower and could only be used on the surface during compaction.

SUMMARY AND CONCLUSIONS

The primary purpose of this study was to evaluate the usefulness of the soil strain gauge system for measuring compaction in the field. The advantages and limitations were sought, and proper techniques for the successful applications were determined.

The wide range of field situations considered in pursuing this objective included materials ranging from unclassified embankment fill to natural gravels and slag, smooth-drum vibratory rollers and sheepsfoot rollers, loose-lift depths from 6 to 60 in., as many as 50 roller passes, a variety of methods of sensor installation, and strains from both primary and secondary compaction with monitoring continued during 9 months in some cases.

The series of field experiments provided not only information on strain gauge performance but also interesting new information on field compaction. Included is the observation that, for normal 6- to 12-in. loose lifts receiving 3 to 6 roller passes, significant additional density increases may occur during secondary compaction, that is, as a result of compaction of succeeding lifts placed on top of the initial lift.

The following conclusions regarding general performance of the instrumentation system are indicated:

1. The sensors may be easily installed with a high probability of successful performance;
2. Meaningful results can be obtained in crushed slag, coarse gravel, and variable till, which are inherently difficult to measure;
3. Independent checks using direct-spacing measurements confirmed the reliability of the electrical readings;
4. For the coaxial configuration, adverse effects due to sensor misalignment, offset, and rotation were shown to be unimportant in almost all cases;
5. The small coplanar strains indicating horizontal changes showed variable trends that could have been a result of offset and rotation effects, but it is equally probable that these trends indicate actual compaction effects; and
6. The precision of long-term readings was on the order of 0.1 percent strain.

A variety of sensor installation techniques were evaluated, and the basic concepts have been summarized in another report (2). The appropriate methods depend on the specific application and the degree of control over the construction operation.

The percentage of vertical strain was shown to be representative of the percentage of density change because the horizontal strains were usually small by comparison. In some cases, a more accurate estimate of density change is obtained if the 3 orthogonal strains (vertical, transverse, longitudinal) are summed. The density change is sufficient information on compaction for many applications. If density is known at any stage of compaction, say initially, then all of the strain readings can be converted to density rather than just to density change.

Based on data from one of the experiments, the error in percentage of density change calculated from the nuclear measurements was 3 times the error in percentage of strain change. Thus, the strain sensors were better able to detect changes in compaction between test sections. However, the difference is even greater if changes between passes at a given point are desired. The strain sensors can readily detect changes of 0.1 percent strain, which corresponds to about 0.1 lb/ft^3 density change, or a factor of 10 smaller than the density methods can be expected to detect.

Examples of application to compaction problems, which seem feasible based on experience in this test program, are as follows:

1. Determine change in compaction with additional roller passes to establish optimum roller efficiency in a particular soil condition;
2. Determine variation of compaction with depth to establish best lift thickness;
3. Determine the effect of compactor parameters such as speed, weight, and tire pressure on amount of compaction and compare the results for a given roller in several types of material;
4. Evaluate adequacy of compaction by comparing change during the application of a proof roller;
5. Provide data on amount of secondary compaction to evaluate the desirability of reduction in the number of passes or applied effort during primary compaction;
6. Monitor changes after compaction to provide an indication of potential instability of the fill;
7. Establish satisfactory compaction procedures for use with materials in which density measurements are not reliable;
8. Determine settlement distribution within a compacted fill by means of a vertical stack of sensors;
9. Evaluate local volume changes of compacted fills caused by changes in moisture and temperature;
10. Observe lateral confinement change due to movements of adjacent structures such as retaining walls and culverts; and
11. Document variability of compaction.

There are also limitations to the use of the strain gauge in compaction studies.

1. In normal field situations, the changes in the top inch or so of material immediately below the compacting element of the roller cannot be realiably measured. That zone is hard to predict for a sheepsfoot roller, and therefore the method may not be feasible for evaluating primary compaction with such rollers.
2. Accurate prediction of density changes may require the determination of 3 strain components if comparison of vertical strains is not sufficient. If the types of compactors are quite different, then all 3 strains may also be needed to ensure proper interpretation.
3. Once sensors are installed, the measurement location is fixed. Information on primary compaction cannot be obtained at other locations after compaction.
4. Dynamic strain measurements during roller passage cannot be obtained closer than 2 to 4 sensor diameters from a part of the roller that influences the magnetic field. For steel-wheeled rollers, this means 8 to 16 in. below the surface with the 4-in. diameter sensors.

The instrumentation system used in this study has evolved from 6 years of research and development, and its feasibility in the field has been demonstrated by the results of the study. Earlier studies demonstrated usefulness in the laboratory. The method is ready for application to appropriate problems. The primary need at this time is the accumulation of experience, and that can only come from use.

ACKNOWLEDGMENTS

Initial encouragement for this study resulted from discussions with W. P. Hofmann and Lyndon Moore of the New York State Department of Transportation. Technical liaison was provided by Peter Houghton, and administrative direction was provided by I. F. Rizzuto, both of the Engineering Research and Development Bureau, New York State Department of Transportation.

Coordination of the project field operations was assumed by Thomas Reamon, a graduate research assistant at the State University of New York at Buffalo. Three other graduate research assistants, Jackson Ho, Louis Garcia-Andion, and James DeCaro, participated in the tests and in the data analysis. Ho was also responsible for initial evaluation of the instrumentation.

The tests in Vicksburg, Mississippi, were made possible through the cooperation of the Waterways Experiment Station, which made available facilities and supporting staff under the direction of R. G. Ahlvin and Cecil Burns. The compactor and technical assistance in those tests were contributed by Rex Chainbelt Company, Milwaukee, through the cooperation of R. M. Strand, and E. Haker, who also participated in the tests.

The study was sponsored by the New York State Department of Transportation and the Federal Highway Administration. The opinions, findings, and conclusions expressed in this publication are those of the author and not necessarily those of the sponsoring agencies.

REFERENCES

1. Selig, E. T., and Grangaard, O. H. A New Technique for Soil Strain Measurement. Materials Research and Standards, Vol. 10, No. 11, Nov. 1970, p. 19.
2. Selig, E. T. Soil Compaction Evaluation With Strain Measurements. Engineering Research and Development Bureau, New York State Department of Transportation, Spec. Rept. 9, Dec. 1971.
3. Truesdale, W. B., and Schwab, R. B. Soil Strain Gage Instrumentation. Proc., Int. Symp. on Wave Propag. and Dyn. Prop. of Earth Mater., Univ. of New Mexico Press, Albuquerque, 1968, pp. 931-941.
4. Morgan, J. R., and Gerrard, G. M. Free Field Measurement of Stresses and Strains in Soils. Proc., Australian Road Research Board, Vol. 4, Pt. 2, 1968, pp. 1747-1760.
5. Selig, E. T., and Ho, J. Retaining Wall Experiment to Evaluate Soil Strain Gage. Jour. Soil Mech. and Found. Div., Proc., ASCE, Vol. 97, No. SM6, Paper 8162, June 1971, pp. 953-957.

NUCLEAR SOIL-MOISTURE CORRELATION

Robert E. Smith, Materials and Research Department, California Division of Highways

Nuclear soil-moisture gauges are commonly used to control the compaction of soil. The nuclear moisture test depends on the moderation, or slowing down, of fast neutrons (emitted from a radioisotope contained in the gauge) by the hydrogen in the soil water. The free or easily evaporable soil water must be controlled in earth construction. However, different soils have varying amounts of other forms of water such as hydrates, interlayer water, and hydroxyl water. Those are not easily evaporable but are detected by the gauge. Also, some soils contain elements that absorb the slow neutrons. This reaction may affect the nuclear moisture test. Consequently, a method must be found of adjusting a gauge calibration determined in the laboratory so that it may be used with the gauge in the field to test a variety of soils. The experimental data were obtained by testing (with 2 nuclear moisture gauges) 4 soil-water systems compacted in large molds. They were prepared at various water contents and included a silica sand, a kaolin clay, a clayey field soil, and an expanded shale. The results of this research indicate that it is satisfactory to assume that the free water calibration curves for various soils differ by a constant that depends on the sum of the effects of structural water and absorbing elements present. The slope of the nuclear moisture calibration curves is satisfactorily established by testing on reference standards of silica sand and water.

•IN THE FALL of 1967, research directed at development of calibration standards for nuclear moisture-density gauges was undertaken by the California Division of Highways. Temporary moisture standards having high and low water contents were prepared by compacting a local river sand in molds cut from steel drums. Before compaction, the sand was allowed to come to air-dry equilibrium moisture. It was then compacted similarly in each of the tubs, and the bulk densities of both were calculated.

One tub was constructed with a piezometer and a plastic tube leading to the bottom so that it could be saturated. This sample was flooded till the free water surface was at the sand surface and all voids were essentially full of water. The amount of water added was measured and checked by weighing the tub and contents before and after. The initial water content of the sand was estimated from oven-dry moisture samples, and as a result the total water content of the saturated moisture standard was known.

The tub containing air-dry sand that had no further water added was used as a low-moisture standard. Subsequent weighing of that sample indicated little change in moisture content. When it was torn down, the top 1 to 2 in. was found to be slightly drier than the greater depths. However, that had a negligible effect on the nuclear moisture tests taken on that sample.

When a calibration curve established by those standards was compared with one (for the same gauge) developed by the use of "oven-dry" field moistures, the two were displaced by about 3 lb/ft^3 of water. That is, the indicated water content of a site was lower when the oven-dry calibration was used than when the sand-water calibration was used. It was very evident, however, that the estimated regression through the field data points was essentially parallel to the laboratory calibration. Because these were developed independently, the conclusion was that the relation between the 2 methods of calibration should be investigated further.

"STRUCTURAL" SOIL WATER

The conclusion was that the observed phenomenon was due to the presence of moisture, especially in the clay minerals, which was not removed in the oven-dry test. The nuclear moisture gauge response is proportional to the hydrogen contained in any form of soil water. In addition to the free water, that may include interlayer water, hydrates, and hydroxyl water. That all of those forms of "structural" soil water are not evaporated at temperatures of 105 to 110 C is easily demonstrated. For example, Nutting reports that the kaolin minerals lose an additional 14 percent by weight (approximately) of hydroxyl water between 400 and 800 C (1, p. 206), with the ensuing destruction of the kaolinite. The number of hydrogen atoms in hydroxyl water is half that of the corresponding quantity of free water molecules. Consequently, the nuclear moisture gauge would respond to the free water equivalent of the hydroxyl water in kaolin (or about 7 percent by weight).

Typical data (estimated from Grim, 8) for some clay minerals are shown in Figure 1. The values are approximate average values and show the trend toward additional water loss at temperatures above 100 C. For the portion of that loss considered to be hydroxyl water, the equivalent free water (half) is given.

Hydrates such as the zeolites and serpentines also contain significant amounts of water that are not driven off by temperatures of 105 to 110 C. Also, Lambe reported that a diatomaceous earth retained significant amounts of water at temperatures above 105 C (2). That is apparently caused by the attractive forces of the very large internal surface area of this soil. That water should be similar in behavior to the bound water of the clay minerals.

THERMAL NEUTRON ABSORPTION

Figure 2 shows moisture correlation data for a nuclear gauge used on Leda clay (3). Nuclear readings versus oven-dry moisture contents of the soil are nearly 6 lb/ft^3 to the right of the reference curve. This is the opposite extreme from the California field-calibration data. Burn's reference curve is based (in part) on silica sand and water standards having known total water content; those standards generally correspond to the temporary California highway standards previously described. Burn speculated that the discrepancy between the 2 calibrations was due to the presence in the clay of iron, which absorbed the neutron flux. He observed, as is apparent in the figure, that the displacement between the 2 curves appears to be a constant for that soil.

DISCUSSION OF CALIBRATION PROBLEM

It has been shown that, if the nuclear gauge is calibrated by oven-dry moisture determinations, it can indicate a water content of field soils as much as ± 6 lb/ft^3 of water from that based on an inert system such as silica sand and water. However, free soil moisture must be controlled in earth construction, and that has been shown to be a variable percentage of the total soil water to which the nuclear gauge responds. Consequently, unless it can be demonstrated that a consistent relation exists between a calibration based on standards of known water content and free water content of individual soils, the users of the gauges are forced to calibrate by field correlation. That is difficult and, in some cases, impossible to do because a sufficient range of data is often not available to establish the slope of the curve with any degree of confidence.

EXPERIMENTAL PROCEDURE

The experimental procedure involved the careful fabrication and testing with nuclear moisture gauges of 4 soil-water systems in large molds: commercial silica sand, commerical kaolin clay, typical clayey field soil, and expanded shale.

The approximate structural water content of the soils was determined on the basis of high-temperature evaporative tests, mineral identification, and differential thermal analysis (DTA). Therefore, the exercise of careful control of the amount of water added made it possible to closely estimate both the free water and total (equivalent) water content of the individual samples.

The physical data concerning the dimensions, volumes, densities, and water contents of all samples tested with the nuclear moisture gauges in the experimental program are given in Table 1. The volumes of the samples were checked to ensure that they were essentially infinite for testing with the gauges.

The top surfaces of most of the samples were protected by a layer of polyethylene plastic. Readings taken with and without the covering indicated that the plastic had a negligible effect on the testing.

Silica Sand Samples

Silica sands obtained from 2 sources were 99.7 to 99.9 percent pure SiO_2. The approximate grading of the sands used is given in Table 2. Four samples were fabricated:

1. Sample A-70 was compacted dry in approximately 2-in. lifts with an electric impact hammer; a plywood disk was used to confine the sand. The sample was provided with a piezometer and a perforated plastic tube so that it could be saturated from within.
2. Sample E-25 was prepared similarly, except that No. 25 sand was used.
3. For sample A-70-200, a ground silica sand (No. 200 flour) was uniformly mixed with No. 70 sand to reduce the void space so that a lower saturated water content was obtained.
4. In sample E-25, the dry silica sand standard was fabricated with No. 25 sand. The moisture content of this sand when initially compacted was hardly detectable. After exposure to the atmosphere in the test area for a period of several months, it gained as much as 0.2 percent moisture.

An attempt was also made to fabricate a partially saturated sample by compacting the moistened sand in increments. Polyethylene plastic was used to prevent migrations of water. However, sufficient water movement occurred in the top layer to affect the gauge readings and made this type of specimen unsatisfactory.

Kaolin Samples

A kaolin clay of high purity was obtained from Ione, California. The physical properties and chemical analysis, according to the producer, are given in Table 3.

An independent analysis of a sample of this clay was made by X-ray diffraction and DTA at the Materials and Research Laboratory. The analysis confirmed that the clay was a typical kaolin and gave little or no indication of the presence of other clay minerals.

High-temperature evaporation tests were conducted with oven-dry samples of the Ione kaolin. The samples lost 0.1 percent by weight between 105 and 400 C and 12.2 percent by weight between 400 and 600 C. The loss in weight was considered to be primarily hydroxyl water, and an equivalent water loss between 105 and 600 C of 6 percent was presumed for the purposes of the study.

Two samples of the kaolin were then similarly prepared in large molds for testing, except that different amounts of free water were added to each. The intent was to obtain as high and as low a water content as possible, with uniform compaction, and not too great a difference in the dry density of the two. The amount of free water added was estimated on the basis of preliminary testing and representative oven-dry samples of the clay taken during compaction. The water contents of the samples were also checked when they were dismantled after the testing was completed. One of the samples (kaolin high) was dried in a 105 to 110 C oven and then retested with the nuclear moisture gauges.

Field Soil Samples

Two samples of a typical field soil were prepared and tested similarly at a high and low free water content. A third field soil sample was fabricated by compacting the material in an oven-dry condition. The grading and chemical data for the soil are given in Table 4.

Figure 1. Approximate water loss of various minerals.

Mineral	Temperature °C: 100 – 200 – 300 – 400 – 500 – 600 – 700 – 800		Structural Water: Total (equiv) H_2O loss
Kaolin Halloysite	Little loss	Approx. 14% by wt. OH^- (equiv. H_2O loss = 7%)	7%
Montmorillonite Smectite	Approx 3% loss inter-layer H_2O	Approx 5% loss OH^- (equiv. H_2O = 2½%)	5½%
Vermiculite	Approx. 8% loss inter-layer, cation hydrates	Approx. 3% OH^- (equiv. H_2O = 1½%)	9½%
Illite (Mica group)	Gradual loss 2% (presumed H_2O)	OH^- loss est. 4½% (equiv. H_2O approx. 2%)	4%
Chlorite	Little loss	OH^- loss approx. 12% (equiv. H_2O = 6%)	6%
Sepolite	Gradual loss to 10% (presumed H_2O)	OH^-, gradual loss to 6% (equiv. H_2O = 3%)	13%

Figure 2. Calibration curve for Leda clay.

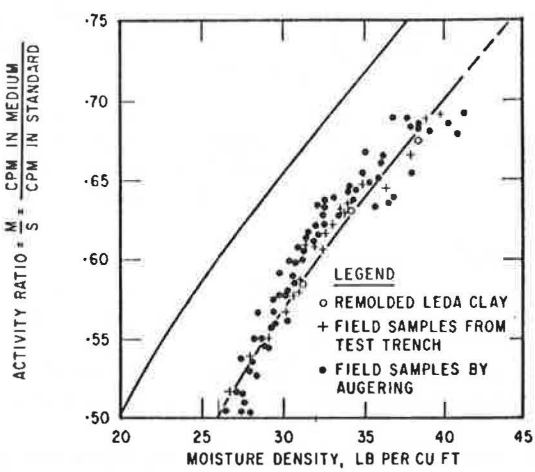

Table 1. Physical data for experimental soil-water samples.

Soil-Water System	Sample	Shape	Least Top Surface Dimension (ft)	Depth (ft)	Volume (ft^3)	Density (lb/ft^3) Wet	Density (lb/ft^3) Dry	Water Content (lb/ft^3) Free	Water Content (lb/ft^3) Struct.[a]	Water Content (lb/ft^3) Total
Silica sand	A-70 wet	Cylindrical	1.87	0.94	2.63	125.4	100.9	24.5	–	24.5
	E-25 wet	Cylindrical	1.87	0.92	2.55	130.2	110.9	19.2	–	19.2
	A-70-200 wet	Cylindrical	1.87	0.87	2.43	123.9	109.6	14.3	–	14.3
	E-25 dry	Cylindrical	1.87	1.19	3.31	–	111.7	–	–	–
Kaolin clay	High	Octagon	1.50	1.17	2.31	97.1	77.9	19.2	4.7	23.9
	Low	Rectangular	1.00	1.50	2.25	80.1	70.7	9.4	4.2	13.6
	High, dry	Octagon	1.5	1.17	2.31	–	77.9	–	4.7	4.7
Field soil	High	Octagon	1.50	1.17	2.31	146.0	131.9	14.1	2.0	16.1
	Low	Rectangular	1.00	1.50	2.25	137.4	129.8	7.6	2.0	9.6
	Dry	Cylindrical	1.87	1.22	3.29	89.9	89.9	–	1.4	1.4
Expanded shale	ES-20.6	Cylindrical	1.87	0.95	2.76	109.2	87.0	22.2	–	22.2
	ES-17.4	Cylindrical	1.87	0.94	2.64	94.4	77.0	17.4	–	17.4
	ES-12.0	Cylindrical	1.87	0.94	2.62	93.8	81.8	12.0	–	12.0
	ES-6.0	Cylindrical	1.87	1.14	3.27	88.2	82.1	6.1	–	6.1
	ES dry	Cylindrical	1.87	1.19	3.29	88.6	88.2	0.4	–	0.4

[a]Equivalent water content.

High-temperature evaporation tests were also conducted on oven-dry samples of the field soil. A loss of 0.5 percent by weight was recorded between 105 and 400 C and 2.2 percent between 400 and 600 C. The loss in weight between 105 and 500 C was assumed to indicate an equivalent water content of 1.5 percent by weight.

Expanded Shale-Sand Samples

Five samples were prepared of an expanded shale-sand. This material is manufactured by expanding sand-sized particles of montmorillonite shale in a rotary kiln heated to temperatures of approximately 2,000 F. The grading of the expanded shale-sand and the manufacturer's chemical analysis are given in Table 5.

Sample ES-20.6 was prepared by compacting and then flooding until it was saturated. The ES-dry sample was left in a dry or "as-compacted" state. The remaining 3 samples were prepared by moistening the shale-sand to intermediate water contents and then compacting. Because of the absorbent nature of the calcined shale, the procedure appeared to work satisfactorily, and little migration of water was discerned during the period of testing. The water contents of several of the shale-sand samples were checked by removing the material in layers and oven-drying the entire increments.

NUCLEAR MOISTURE DATA

The soil samples were not necessarily fabricated or tested with the nuclear gauges in the order presented, nor was it possible to retain all samples so that they could be tested concurrently. That was compensated for by reading all available samples as each new sample was being tested. The average of those readings was then plotted against sample free water (Fig. 3) and against the estimated total water content (Fig. 4).

Two nuclear soil gauges were used during this study. Gauge A is an older unit that has been found to be relatively stable during an extended period of time. The source contained in this gauge is 4.5-mC radium 226-beryllium. Gauge B is of more recent manufacture and contains a 50-mC americium 241-beryllium fast neutron source.

Free Water Correlation Data

Figure 3 shows the response of gauges A and B plotted against the free water content of the samples. The curves are drawn by visual "best fit." For gauge A, the calibration curves for the 4 soil-water systems are essentially parallel, except for the expanded shale at the lower water contents. The readings taken with gauge B indicate a greater variation in the slope of the individual calibration lines.

The data for the expanded shale-water system reflect a high degree of neutron flux absorption. A report by the Oklahoma Department of Highways showed a similar datum point for an expanded shale-water sample tested (4, p. 89). The chemical analysis of the shale-sand indicates the presence of about 6 percent of iron and potassium in the material; that amount does not seem sufficient to cause the amount of absorption shown.

The oven-dry expanded shale sample (ES dry) plotted very closely to the dry silica sand sample (E-25-D) (Fig. 3). This apparently means that a certain level of activity is required before the capacity of the material to absorb thermal neutrons becomes saturated. At some water content, this absorptive capacity of the soil begins to be satisfied. Thereafter, the production of thermal neutrons with change in water content is almost as though the absorptive elements were not present. Above that critical water content, the calibration curves for soils with absorptive elements for thermal neutrons appear to be reasonably parallel to the silica sand calibration curve.

That the net effect of the presence of structural water and slow neutron-absorbing elements in a soil is a calibration constant is undoubtedly an oversimplification. However, it is concluded that the slope of a calibration curve determined by using standards of silica sand and water should be satisfactory for nuclear gauge moisture determinations on most soils. An exception may have to be made for those containing highly absorptive elements, especially at water contents below 6 lb/ft^3 of water. It is not known to what degree such materials may be encountered in soils used in highway construction.

Table 2. Grading for silica sand.

Item	E-25	E-85	No. 200	A-70
Fineness	25.88	84.42	–	65
Sieve, percent retained				
20	2.2			
30	38.6			
40	57.6	0.0		06
50	1.4	2.4		3.9
60				9.3
70	0.2	10.0		20.5
80				22.1
100		45.0		31.2
140		20.0	1.0	11.6
200		11.0	4.0	0.7
270		2.4	6.0	
325		1.0	9.0	

Table 3. Physical and chemical data for Ione kaolin.

Property	Value
Physical	
Specific gravity	2.60
Moisture (max), percent	0.5 to 1.0
Particle size, percent	
-2 μm	50 to 55
+5 μm	20 to 25
pH	4.5 to 5.5
Water of plasticity, percent	31.9
Average particle size, μm	2.2
Chemical	
Silica, percent	45.0 to 47.0
Alumina, percent	37.5 to 39.0
Iron oxide, percent	0.3 to 0.5
Titanium dioxide, percent	1.5 to 2.0
Ignition loss, percent	13.0 to 14.0

Table 4. Grading and chemical data for field soil.

Item	Value[a]	Item	Value[a]
Sieve, percent passing		Mineral, percent	
3/4	100	Quartz	25 to 30
1/2	84	Feldspar	10 to 15
3/8	73	Chlorite	10 to 15
4	52	Mica	5
8	41	Hornblende	5
16	31	Miscellaneous clay	5 to 10
30	23	Talc	2 to 3
50	18	Augite	2 to 3
100	15	Other crystalline	5
200	13	Amorphous	15
5 μm	8		
1 μm	6		

[a]Estimated from X-ray diffraction data.

Table 5. Grading and chemical data for expanded shale-sand.

Item	Value	
Sieve, percent passing	Basalt Rock Co.	M and R
4	99	
8	82	82.6
12		52.6
16	56	
30	36	33.3
50	23	22.1
100	12	13.5
200		6.5
Chemical	Raw Shale	Calcined Shale
SiO_2	59.2	62.8
Al_2O_3	20.0	21.7
CaO	2.6	3.2
Fe_2O_3	3.3	4.4
MgO	2.7	3.3
Na_2O	2.6	2.6
K_2O	1.6	1.6
H_2O	8.0	0.0
Ignition loss	Trace	0.4

Figure 3. Nuclear free moisture correlation test data.

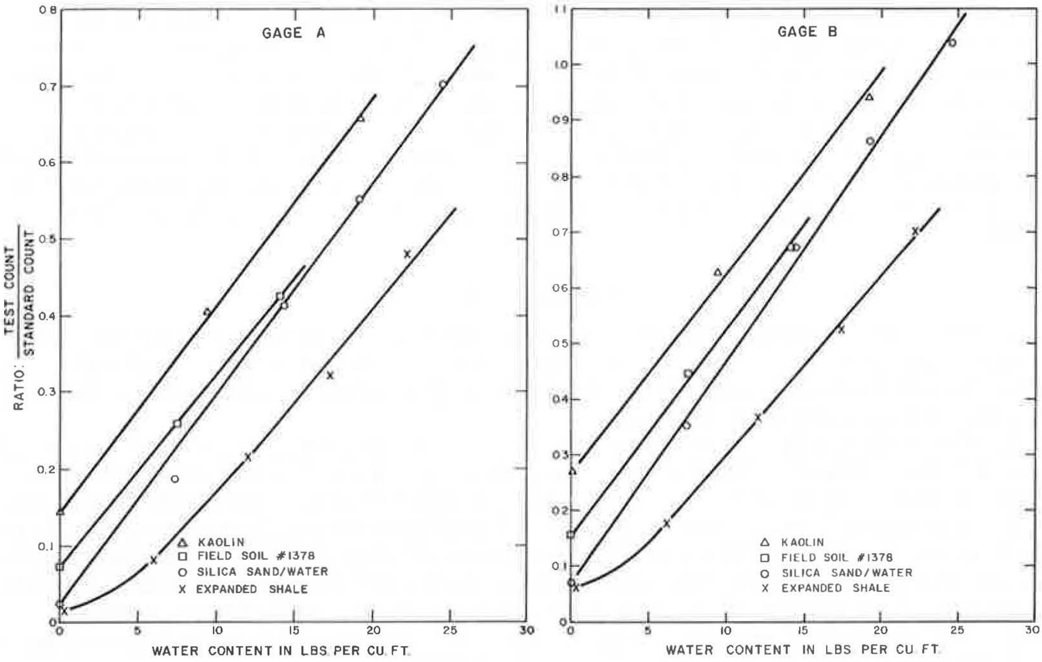

Figure 4. Nuclear total moisture correlation test data.

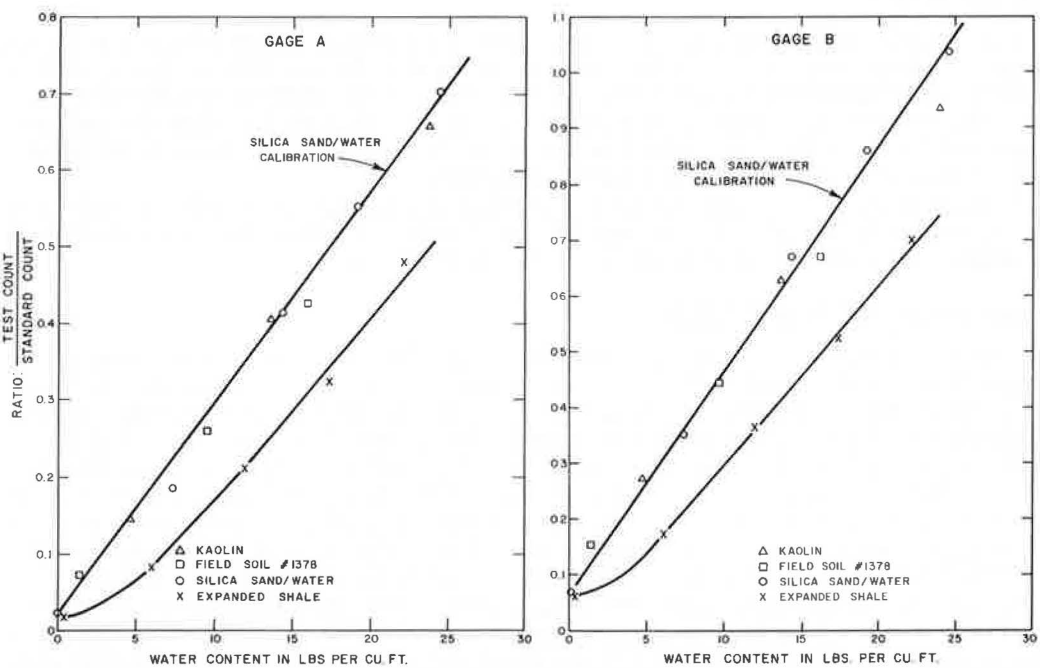

Total Water Correlation Data

Figure 4 shows the average nuclear gauge readings plotted with respect to the estimated total water content of the samples. Most of the moisture data for the clay soils now plot either on or to the right of the silica sand calibration curve. It is concluded that nuclear instruments for measuring moisture do respond to the structural water as well as to the free water. However, the effect of the hydroxyl water does not appear to be directly porportional to the hydrogen content. This is to be expected because the bonding of the hydrogen atom to the soil minerals probably reduces its capacity to thermalize the fast neutrons emitted by the radioisotope in the gauge (5, p. 548; 6, p. 347).

CONCLUSIONS

1. The nuclear moisture gauges respond to the total water content of a soil. That includes bound or adsorbed water, interlayer water, hydrates, and hydroxyl water. A water content estimated on the basis of an oven-dry moisture determination reflects only the free or easily evaporable water.
2. For a given water content, the presence of slow neutron-absorbing elements will decrease the response of the nuclear moisture gauge. Except at low water contents, however, the presence of the absorbing elements appears to be a calibration constant.
3. The change in soil water during normal construction activities occurs almost entirely in the free water. The results of this research indicate that it is satisfactory to assume that the free water calibration curves differ only by a constant, which depends on the sum of the effects of the structural water and absorbing elements present.
4. The slope of the nuclear moisture calibration curves is satisfactorily established by testing on reference standards of silica sand and water.

IMPLEMENTATION

"Offset" Method

For specific soils, where an equivalent oven-dry moisture calibration curve for the nuclear gauge is desired, a moisture sample is taken at the site of a nuclear moisture reading. The density of the location must be determined by nuclear or other means. The oven-dry moisture in lb/ft^3 of water is calculated and plotted against the nuclear gauge moisture reading. A calibration curve for that soil is drawn through the point and parallel to the sand-water reference calibration.

This procedure has 2 disadvantages: (a) It is only good for the particular soil, and (b) any errors in the estimates of moisture or density are reflected in the calculated moisture. An alternate and preferred method is discussed.

"Approximate Wet-Weight" Method

A practical method of compaction control is possible; it uses only a wet density correction based on the slope of the moisture calibration curve. The procedure is especially applicable to structural section materials, for which it is often possible to preestablish a satisfactory compaction standard. The concept is similar to that of the "wet-weight" method of compaction control used by California (7, 216-F) and others. This procedure is based on expressing the wet density of a soil and the laboratory control density in terms of the same moisture content. The following example contains a slight approximation, but the percentage of relative compaction is usually within 0.5 percent of that calculated on the basis of the "exact" wet- or dry-weight method.

Suppose that it has been established that a certain soil should have a wet density of 135 lb/ft^3 at some definite (but unknown) water content. This unknown water content is that contained in the material when it was obtained for the laboratory compaction testing. Suppose also that a nuclear moisture gauge had been used to test the location where the soil was obtained at the time it was removed, and the water content was x. At a later time, a site with similar soil is tested and found to have a wet density of 140 lb/ft^3 and water content of $x + 3$. The wet density of the site in terms of the water content at which the control had been established is 140 - 3 or 137 lb/ft^3. This equivalent wet density is greater than the 135 lb/ft^3 previously established as a minimum control density. Thus, if the slope of the nuclear moisture calibration curve is correct, it has been found that the density of the site is satisfactory without its actual water content being known.

ACKNOWLEDGMENTS

This work was accomplished in cooperation with the Federal Highway Administration. Appreciation is extended to Dale Sathre and Frank Champion, who performed the many and sometimes laborious technical operations with care and precision. The contents of this report reflect the views of the author who is responsible for the facts and the accuracy of the data presented. The contents do not necessarily reflect the official views or policies of the California Division of Highways or of the Federal Highway Administration; nor does the report constitute a standard, specification, or regulation.

REFERENCES

1. Nutting, P. G. Some Standard Thermal Dehydration Curves of Minerals. In Shorter Contributions to General Geology, U.S. Geological Survey, Prof. Paper 197-E, 1941-42, pp. 197-217.
2. Lambe, T. W. How Dry Is a Dry Soil? HRB Proc., Vol. 29, 1949, pp. 491-496.
3. Burn, K. M. Calibration of a Neutron Moisture Meter in Leda Clay. Canadian Geotechnical Jour., Vol. 1, No. 2, March 1964, pp. 94-103.
4. LeFevre, E. W., and Manke, P. G. A Tentative Calibration Procedure for Nuclear Depth Moisture/Density Gages. Highway Research Record 248, 1968, pp. 82-90.
5. Preiss, K., and Grant, P. J. The Optimization of a Neutron Scattering Water Content Gauge for Soils or Concretes. Jour. Scientific Instruments, Vol. 41, 1964, pp. 548-551.
6. Preiss, K. Relation Between the Energy of Radiation and the Influence of Soil Composition in Radioisotope Methods of Water Content and Density Measurement. Proc., 3rd Asian Reg. Conf. on Soil Mech. and Found. Eng., Haifa, 1967, pp. 345-347.
7. Materials Manual: Testing and Control Procedures. California Division of Highways, Vol. 1.
8. Grim, R. E. Clay Mineralogy, 2nd Ed. McGraw-Hill, New York, 1968.

SIMULATION OF THE ROAD-CORRUGATION PHENOMENON

J. G. Riley, Department of Agricultural Engineering, University of Maine at Orono; and
R. B. Furry, Department of Agricultural Engineering, Cornell University

A mathematical model was formulated to simulate the phenomenon of washboarding on unpaved roads. Both the vehicle and the road components were treated as spring-mass-damper assemblies. A digital computer program was written to solve the equations of motion of the system; displacement forcing functions represented irregularities in the path of a moving wheel. The program was executed with varying road and vehicle characteristics, and thus the relations among those primary characteristics and washboard presence and dimensions were established and then verified by physical model tests in the laboratory. In both the simulation and the physical tests, the primary and secondary variables were expressed as dimensionless ratios. Results showed that vehicle weight, tire pressure, and vehicle speed affected primarily the wavelength of the corrugations but that there were maximum or minimum values of those parameters above or below which corrugations would not occur. Results also showed that, for the particular surface materials used, washboarding occurred more readily in a material with a relatively high specific damping capacity and that this property was related to particle shape, effective size, and uniformity coefficient.

•UNPAVED roads subjected to vehicular traffic can, under certain circumstances, suffer from a phenomenon known as washboarding or corrugation, whereby the initially flat road surface becomes deformed into a regular pattern of waves perpendicular to the longitudinal axis of the road. Although the amplitude of the waves is generally only a few inches, the effect on vehicles passing over them is severe, and the usefulness of roads so affected is greatly impaired.

There have been many reports on the occurrence and characteristic forms of washboarding, but there is no one accepted explanation concerning the cause of the problem. Existing theories contain much contradictory information and generally lack solid evidence that would encourage support. It was hypothesized that, if the phenomenon could be simulated mathematically and verified by experimentation, then the mechanism could be explained and the causative factors identified. Thus, a rational basis would be established for work related to practical means of preventing or curing the problem. So that the model developed would be as general as possible, it was decided that the study should attempt to identify all possible pertinent variables and present results in terms of dimensionless groups of those variables

MATHEMATICAL MODELING OF THE ROAD-VEHICLE SYSTEM

The system was treated as a pneumatic-tired wheel running along an initially flat surface layer of granular material on a rigid base. The vehicular component was represented mathematically as a spring-mass-damper system, with a linear spring rate and velocity-dependent damping. Modeling of the loose surface material is a more complex problem because this model must eventually be tied in, from a behavioral aspect, with the vehicle model.

Classical load-sinkage studies for rolling wheels and tracks in soils have always assumed "static" (i.e., slow) loading conditions (2, 4). Physical observations of washboarding, however, showed that it is a phenomenon involving impact loading and that velocity is indeed critical. If rate of loading is to be considered, then, according to

Bekker (1), the soil forces produced by an impact may be thought of as the sum of the static force and additional forces resulting from viscocity and acceleration of the soil mass. For a plate-sinkage test, as a first approximation,

$$F_s = f_1(Z) + f_2(Z, \mathring{Z}) + F_3(Z, \ddot{Z}) \tag{1}$$

where

F_s = soil force acting on the plate,
Z = penetration of the plate,
$\mathring{Z}$ = velocity of the plate, and
$\ddot{Z}$ = acceleration of the plate.

It is obvious from this equation that the soil mass is, in the broadest sense, being treated as a spring-mass system with damping. Such a representation of soil has been used in the study of earthquakes and wave propagation for many years, generally because of the difficulty of describing dynamic behavior satisfactorily by any other method.

Rickman (10) outlines techniques for describing materials by means of a spring and dashpot, representing respectively the elastic and viscous components. To accurately describe the behavior of nonhomogeneous soils requires the incorporation of large numbers of spring and dashpot pairs (6, 7, 14); but for a single homogeneous layer of granular material resting on a rigid base, it is reasonable to use a single spring-dashpot pair. The nonlinearity of static load-deflection curves for any granular material, however homogeneous it may be, necessitates the use of empirical load-deflection data to represent the nonlinear spring; that precludes any possibility of an explicit analytical solution to the problem but makes for a much simpler model.

If the mass of soil accelerated is to be considered as a contributing factor to total soil reaction force, then some means of representing that soil mass must be established. Because the soil under the wheel is being treated as a spring-dashpot pair, then the effective mass of that soil will be calculated in the same way that the effective mass of a spring is computed. If the analysis described by Phelan (9) is followed, the accelerated mass of soil will be represented in the model by one-third of the mass under the contact patch of the tire, as determined by the area of this contact patch, the depth of material, and the material's mass density.

The models for the vehicle and road surface are combined in the composite model that is represented as a 2-deg-of-freedom system and shown in Figure 1.

Although the wheel is in contact with the road, the system is governed by the following equations:

$$m_1\ddot{x}_1 = k_1(x_2 - x_1) + c_1(\dot{x}_2 - \dot{x}_1) \tag{2}$$

$$m_2\ddot{x}_2 = k_1(x_1 - x_2) + c_1(\dot{x}_1 - \dot{x}_2) + k_2(y - x_2) + c_2(\dot{y} - \dot{x}_2) \tag{3}$$

for $(x_1 - x_2) \le \delta_{st}$, where δ_{st} is static tire deflection.

When the wheel leaves the surface, it moves in a trajectory whose path, neglecting air resistance, is governed by

$$\dot{x}_1 = \dot{x}_{1p} - gt \tag{4}$$

for $(x_1 - x_2) > \delta_{st}$, and where

$\dot{x}_{1p}$ = vertical velocity of projection,
g = acceleration due to gravity, and
t = time measured from the instant of projection.

In the horizontal plane, as the vertical reaction force on the tire changes, so will the effective rolling radius. For a towed wheel tending to rotate at constant angular velocity, this results in slippage i defined by

$$i = 1 - \frac{R}{R_{st}} \tag{5}$$

where

R = effective rolling radius, and
R_{st} = static rolling radius.

If the tire contact patch length is L and if the tire perimeter rolls out a distance L, then the axle of the wheel moves a distance L(1 - i), and the tire contact patch moves relative to the ground a distance -iL, where motion is forward, i.e., skid. Motion of the contact patch on the ground results in horizontal shear of the soil, which in turn results in vertical sinkage. Bekker showed that the relation between horizontal and vertical loads and the corresponding deformations could be expressed by

$$\frac{\tau_{max}}{p - p_{cr}} = \frac{J}{Z_J} \tag{6}$$

where τ_{max}, the maximum shear stress, is given by

$$\tau_{max} = c + p \tan \phi \tag{7}$$

and

p = vertical load per unit area,
c = cohesion of the soil,
ϕ = angle of internal shearing resistance,
J = horizontal deformation, and
Z_J = vertical deformation due to horizontal deformation only.

p_{cr} is Terzaghi's (12) bearing-capacity value defined semi-empirically as

$$p_{cr} = cN_c + \gamma[N_q (Z_s + Z_J) + \tfrac{1}{2} b N_\gamma] \tag{8}$$

where N_c, N_q, and N_γ are dimensionless ratios depending only on ϕ, and where

γ = specific weight of the material,
b = width of the contact patch, and
Z_s = sinkage due to vertical load only.

Combining Eqs. 6, 7, and 8 yields

$$Z_J = \frac{J[p - cN_c - \gamma (N_q Z_s + \tfrac{1}{2} b N_\gamma)]}{c + p \tan \phi + \gamma N_q J} \tag{9}$$

Thus, total vertical deformation Z_o is defined by

$$Z_o = Z_s + Z_J \tag{10}$$

APPLICATION OF DIMENSIONAL ANALYSIS

Concurrent with the mathematical modeling of the phenomenon, all possible relevant vehicle and surface material parameters were identified and arranged in dimensionless groups, according to the laws of dimensional analysis, in order to facilitate an understanding of the specific effects of a particular variable, both in the mathematical solution and in tests on the physical model.

Vehicle characteristics are fairly easily identified, consisting of the mass of the wheel, the tire spring rate and damping coefficient, tire width and geometry, and vehicle speed. Identification of pertinent surface material characteristics is more difficult because, in general, dynamic soil properties have not been successfully defined. The most complete listing of basic properties is given by Hansen (5). The discarding of variables not applicable to this situation results in the list given in Table 1.

The secondary variables, wavelength and amplitude of the washboarding, may be expressed as some unknown function of the primary variables.

$$L = f_1 (W, k_1, \zeta_t, b, d, v, g, n, t, \gamma, c, \phi, s, C_u, \zeta_s, \sigma, \lambda, h) \tag{11}$$

$$A = f_2 (W, k_1, \zeta_t, b, d, v, g, n, t, \gamma, c, \phi, s, C_u, \zeta_s, \sigma, \lambda, h) \tag{12}$$

A dimensional analysis then yields the following results:

$$\frac{L}{s} = F_1 \left(\frac{W}{cs^2}, \frac{k_1}{cs}, \zeta_t, \frac{b}{s}, \frac{d}{s}, \frac{v}{g^{1/2} s^{1/2}}, n, \frac{t}{s}, \frac{\gamma s}{c}, \phi, C_u, \zeta_s, \sigma, \frac{\lambda}{s}, \frac{h}{s} \right) \tag{13}$$

$$\frac{A}{s} = F_2 \left(\frac{W}{cs^2}, \frac{k_1}{cs}, \zeta_t, \frac{b}{s}, \frac{d}{s}, \frac{v}{g^{1/2} s^{1/2}}, n, \frac{t}{s}, \frac{\gamma s}{c}, \phi, C_u, \zeta_s, \sigma, \frac{\lambda}{s}, \frac{h}{s} \right) \tag{14}$$

These dimensionless groups were used to guide the physical test procedure in the evaluation of the mathematical model and in the investigation of the relative contribution of certain variables to the occurrence of form of washboarding. A listing of these groups or pi terms is given below:

$\pi_{1a} = L/s$	$\pi_4 = \zeta_t$	$\pi_8 = n$	$\pi_{12} = C_u$
$\pi_{1b} = A/s$	$\pi_5 = b/s$	$\pi_9 = t/s$	$\pi_{13} = \zeta_s$
$\pi_2 = W/cs^2$	$\pi_6 = d/s$	$\pi_{10} = \gamma s/c$	$\pi_{14} = \sigma$
$\pi_3 = k_1/cs$	$\pi_7 = v/(g^{1/2} s^{1/2})$	$\pi_{11} = \phi$	$\pi_{15} = \lambda/s$
			$\pi_{16} = h/s$

A substantial number of parameters required definition, and that was accomplished by separate testing procedures described in detail by Riley (11). Table 2 gives measured properties of the 3 sands used in the tests. Cohesion and angle of shear were measured with a torsional shear device; effective size and coefficient of uniformity were found by performing a mechanical analysis for each sand; and dumping capacity was measured from the decay of free vibrations for the sand contained in a rubber membrane and subjected to an instantaneous loading condition.

COMPUTER SIMULATION AND PHYSICAL TEST PROGRAM

The mathematical model of the phenomenon allows for prediction of road profile changes as a function of a large number of variables, the values for some of which must be introduced as empirical data. The process of washboarding is a multipass phenomenon; therefore, for prediction of the road profile after a number of passes, the profile resulting from one pass of the wheel becomes the input profile for the next pass and so on. Because of the nonlinearities and the semi-empirical nature of the model, an analytical solution is impossible, and a digital computer solution using numerical methods must be employed.

The physical model constructed in the laboratory consisted of a 6-ft diameter circular track around which a small pneumatic-tired wheel was propelled by a rotating arm driven from the center of the track by an electric motor and reduction gearbox. A schematic diagram of the apparatus is shown in Figure 2. Tests were made on this model with the same values for the variables as those used for computer input. Washboard amplitude and wavelength from peak to peak were measured. Experimental data from these physical tests were then plotted on the graphs obtained from the computer simulation for comparison of actual and predicted results. The flow chart for the simulation, along with a FORTRAN IV program listing and typical prediction model output, is given by Riley (11).

RESULTS AND DISCUSSION

Figure 3 shows the computer prediction of the surface profile after the third, sixth, ninth, and twelfth passes of the wheel. Values for the system variables for this test

Figure 1. Schematic diagram of road-vehicle system.

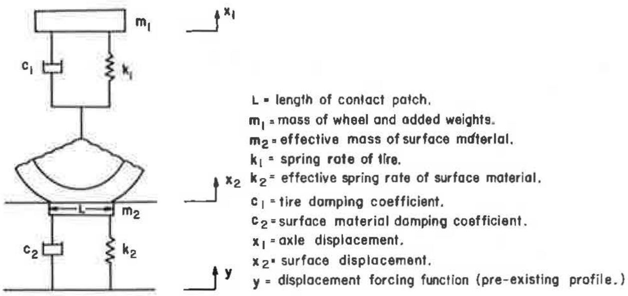

Table 1. Pertinent quantities for road and vehicle.

Variable	Symbol	Units	Dimensions[a]
Secondary			
Wavelength of washboarding	L	Ft	L
Amplitude of washboarding	A	Ft	L
Primary			
Total static weight on wheel[b]	W	Lb	F
Tire spring rate	k_1	Lb/ft	FL^{-1}
Tire damping capacity	ζ_t	—	—
Tire width	b	Ft	L
Tire diameter	d	Ft	L
Vehicle velocity	v	Ft/sec	LT^{-1}
Acceleration due to gravity	g	Ft/sec^2	LT^{-2}
Number of passes	n	—	—
Surface material layer thickness	t	Ft	L
Specific weight	γ	Lb/ft^3	FL^{-3}
Apparent cohesion	c	Lb/ft^2	FL^{-2}
Angle of shearing resistance	ϕ	—	—
Effective size	s	Ft	L
Coefficient of uniformity	C_u	—	—
Material damping capacity	ζ_s	—	—
Particle shape	σ	—	—
Length of initial irregularity	λ	Ft	L
Height of initial irregularity	h	Ft	L

[a]Basic dimensions used in this study are F, force; L, length; and T, time.
[b]Including weight of tire, rim, and suspension components.

Table 2. Measured properties of test sands.

Sand	σ	s (mm)	C_u	ζ_s	c (lb/in.^{2})	ϕ (deg)	γ (lb/ft^3)	N_c	N_q	N_γ
A	Angular	0.045	2.2	0.8	0.1	31	82.2	40	24	23
B	Spherical	0.310	1.4	0.2	0.1	26	93.0	27	15	13
C	Angular	0.080	1.7	0.3	0.1	28	78.9	33	18	19

Figure 2. Schematic diagram of test facility.

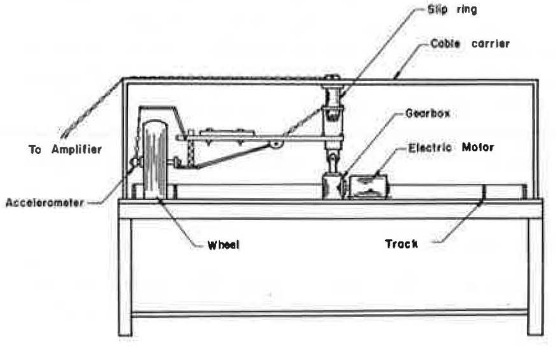

Figure 3. Computer prediction of developing profile.

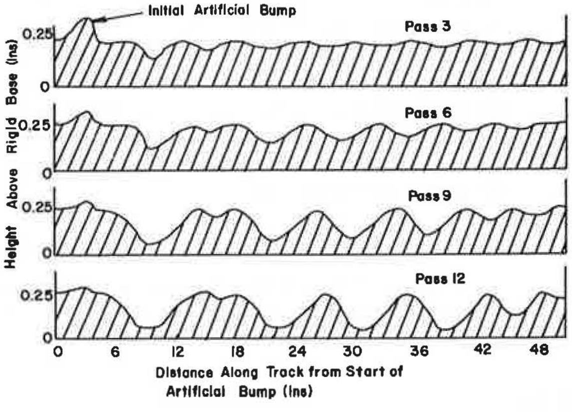

are listed below:

$W = 10.25$ lb	$d = 0.83$ ft	$\gamma = 82.2$ lb/ft^3	$C_u = 2.2$
$k_1 = 2{,}736$ lb/ft	$v = 5$ ft/sec	$c = 14.4$ lb/ft^2	$\zeta_s = 0.8$
$\zeta_t = 0.17$	$g = 32.2$ ft/sec^2	$\phi = 31$ deg	σ = angular
$b = 0.25$ ft	$t = 0.0208$ ft	$s = 0.00015$ ft	$\lambda = 0.33$ ft
			$h = 0.0208$ ft

After only 3 wheel passes, washboarding is present for a considerable distance beyond the initial irregularity; further passes amplify the corrugations while simultaneously shifting the whole pattern in the direction of the wheel's travel. By about the ninth pass, a steady-state amplitude and wavelength condition is reached, after which further passes merely cause a continued forward migration of the developed pattern.

Figure 4 shows a comparison of the predicted and measured profiles for the third and ninth passes of this first test; the values for the various parameters are the same as those given above. There is close agreement between predicted and experimental results, even to the duplication of the first deep depression, the second small one, and the flattening out of the initial irregularity.

Initial qualitative tests on the physical model led to the identification of certain vehicle parameters as having marked effects on the nature of the corrugations, and the second part of the computer simulation involved the study of some of those effects. The particular parameters chosen were tire pressure, weight on the wheel, and vehicle speed. Values for those were varied independently and read into the computer; sufficient wheel passes were made so that the steady-state condition was reached; and the resulting output profile was then interpreted simply as 2 numerical values representing amplitude and wavelength. For a particular tire inflation pressure, i.e., with π_3 constant, the wavelength of the corrugations decreases linearly with increasing weight on the wheel up to a certain weight, after which the decrease becomes essentially exponential. Similarly, under the conditions of testing, for tire inflation pressures between 10 and 30 lb/in.^{2}, washboard wavelength decreases linearly with increasing tire spring rate for constant weight on the wheel. The 3-dimensional representation shown in Figure 5 gives a qualitative description of the relations between those particular pi terms within the given limits. As a generalization, one can say, with all other factors constant and within the range of testing, that high tire pressure and heavy weight on the wheel produce washboarding with a short wavelength and that low pressure and light weight yield a longer wavelength.

Figure 6 shows that, all other parameters being constant, wavelength increases essentially linearly with vehicle velocity within the range of testing, a predictable result and one that agrees completely with the work of other investigators (3, 8).

For given surface material characteristics, if washboarding occurred at all, it did so through wide variation of tire pressure, weight on the wheel, and wheel speed; and its wavelength was directly related to values of those parameters. However, there were certain limiting values for them below or above which washboarding did not occur.

If washboard amplitude, expressed as the pi term A/s, is plotted against the vehicle pi terms, then it is reasonable to select a value for A/s above which washboarding is considered to be present. The value chosen in these tests was A/s = 100, a figure that represented the approximate point where washboarding became readily visible to the naked eye. The independent pi terms are then plotted against one another to show the cutoff points and, thus, define an area within which any combination of the 2 plotted dimensionless variables will result in washboarding. If this is done with 3 independent pi terms, the result is a solid defined region within which washboarding will occur for the given tire, surface, and test conditions.

Results of that procedure are shown in Figure 7. Translated into practical terms, they show, for example, that for this physical system, with all other parameters constant, washboarding will not occur below a vehicle speed of 3.2 ft/sec ($\pi_7 = 46.41$), above a wheel weight of 30 lb ($\pi_2 = 95.59 \times 10^6$), or below a tire spring rate of 100 lb/in. ($\pi_3 = 56.45 \times 10^4$). The lower limit of wheel weight and the upper limit of tire pressure, both expressed as pi terms, are not in fact cutoff points but merely the limiting values

Figure 4. Comparison of measured and predicted profiles.

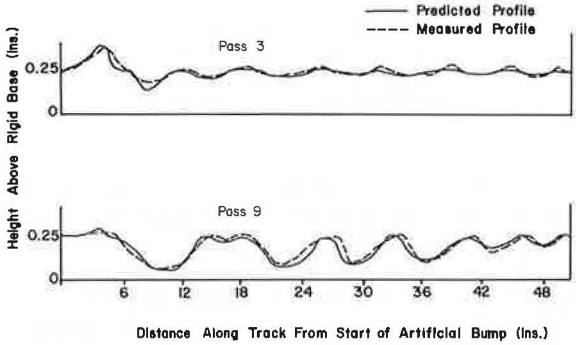

Figure 5. Wavelength as a function of wheel weight and tire inflation pressure, expressed as dimensionless ratios.

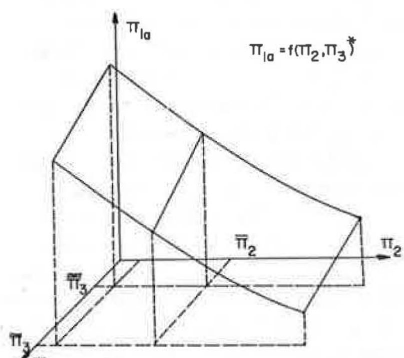

Figure 6. Wavelength as a function of wheel weight and vehicle speed, expressed as dimensionless ratios.

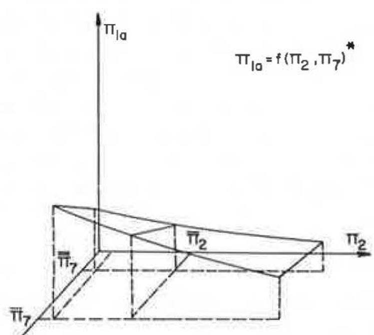

Figure 7. Washboard occurrence as a function of wheel weight, vehicle speed, and tire inflation pressure, expressed as dimensionless ratios.

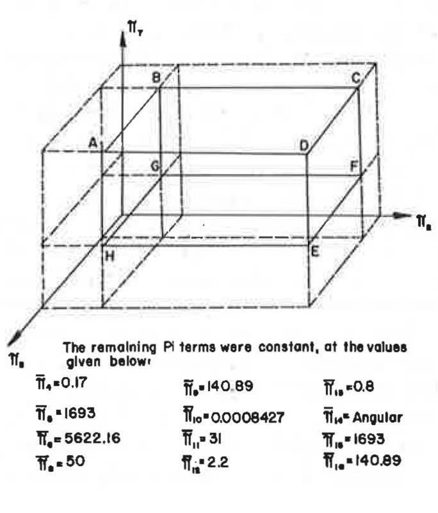

for which experimental data were taken (i.e., beyond the resultant pi term values, washboarding certainly might occur; but since tests were not run for verification, that fact cannot be stated categorically).

These results indicated that the proposed mathematical model provides a good representation of the phenomenon and leads to an understanding of the effects of the vehicle characteristics on the form of the washboarding. It is now appropriate to consider how surface material characteristics influence the phenomenon, especially the reason for causing the occurrence of washboarding in one material but not in another.

Two of the test sands, A and B, showed completely different behavior in that with all other parameters constant one washboarded markedly and the other did not do so at all. Both sands had approximately the same angle of internal shearing resistance ϕ and cohesion c and, therefore, about the same resistance to horizontal shear but widely differing vertical load-deformation curves and damping capacities. When the wheel lands after a bump, however small, there is a slip-sinkage effect. Both sands deform to the same extent because of this; but then, as the wheel rides up the bump resulting from this sinkage, different behavior results. Sand B, with a low damping capacity ($\zeta_s = 0.2$), is deformed by the vertical tire forces so that the wheel is not reprojected into the air but merely continues on the level, forming a flat rut. Sand A, however, with a high damping capacity ($\zeta_s = 0.8$), offers higher resistance to the dynamic vertical forces so that the bump is not totally flattened and the tire is projected into the air to continue the propagation process.

If the measured properties of the sands given in Table 2 are considered, it is seen that, proceeding from sand A through C to B (i.e., yielding washboarding, slight washboarding, and no washboarding respectively), the decrease in damping capacity is accompanied by a decrease in uniformity coefficient and an increase in effective size. That is in agreement with the work of Tschebotarioff and McAlpin (13), who found that low damping capacity was associated with poor gradation for certain sands. It would appear then that materials with a low modulus of sinkage and low damping capacity are incapable of supporting vehicle-induced corrugation and that those characteristics are related to gradation.

However, the susceptibility of some uniform materials to washboarding indicates that gradation alone is not the deciding factor but that some other geometric property is important. For these tests, the geometry of each sand was summarized by σ, s, and C_u. Although this would seem to be an intuitively reasonable method, for a full understanding of the reason for different materials having different damping capacities and, thus, different washboard supporting capabilities, further study is required to identify relevant basic soil properties that would more accurately describe the material.

SUMMARY AND CONCLUSIONS

A mathematical model was constructed to simulate the phenomenon of washboarding on unpaved roads. The road-vehicle system was modeled as a 2-deg-of-freedom mass-spring-damper system, the vertical vibrations of which were described by 2 second-order differential equations. Horizontal displacements were calculated from the change in tire rolling radius and soil mechanics slip-sinkage theory. A digital computer program was written to solve those equations and thus predict the changes in road profile as the wheel rolls along the road.

Varying road and vehicle characteristics were used as input to the program, and the relations between primary vehicle characteristics and washboard presence and dimensions were calculated and verified by physical model tests in the laboratory. For a particular wheel, the vehicle weight, tire inflation pressure, and speed affect primarily the wavelength of the washboard, and amplitude is a function mainly of the loose layer thickness. There were, however, maximum or minimum values of the vehicle parameters above or below which corrugations would not occur. As far as the characteristics of the loose surface layer are concerned, it was shown that for the 3 sands tested washboarding occurred more readily in the well-graded sand, which had a higher damping capacity and greater resistance to dynamic vertical deformation than the less well-graded sands, even though the soil strength parameters of cohesion and angle of internal shearing resistance were approximately the same.

Even though that was a theoretical analysis, it indicates conditions that would not be favorable to washboard formation in the real world. Concerning the vehicle, all that can be recommended practically is that vehicle speeds be kept low on roads proven to be susceptible to corrugation; high wheel weight aids prevention, but that would not seem to be a feasible method in practice. Concerning road materials, if it were possible to increase shear strength to prevent or reduce horizontal shear, or decrease damping capacity so that the bumps would not withstand dynamic wheel forces, then washboarding would not form.

Shear strength can be increased sufficiently to prevent washboarding by paving or asphalting the road for an adequate depth or more practically by increasing cohesion either by application of a binder or by use of a well-graded material with a reasonable proportion of clay. Low specific damping capacity can be most easily achieved, at least in sand, by using a material with little gradation, i.e., having a uniform particle size; however, such a material, although not sustaining washboarding, will allow high wheel sinkage and cause high rolling resistance. It is, therefore, a cure of questionable value. Scraping down and flattening existing washboarding is at best a temporary measure only and at worst an exercise in futility; for, if the road surface material is conducive to the formation of corrugations, then under wheeled traffic the flat surface represents an unstable condition. If the corrugations are merely scraped flat, the road will simply begin to washboard again until the stable corrugated form is reached once more.

Considering the millions of miles of unpaved roads that are susceptible to washboarding, any selection of special road surface material or treatment of existing material must be considered from an economic viewpoint; there is certainly no simple, cheap, and effective means of controlling the problem.

REFERENCES

1. Bekker, M. G. Off the Road Locomotion. Univ. of Michigan Press, Ann Arbor, 1960.
2. Bernstein, R. Probleme zur experimentallen Motorpflugmechanik. Vol. 16, Munich, 1913.
3. Dana, H. J. Formation of Washboards in Gravel Highways. HRB Proc., Vol. 9, 1929, pp. 186-208.
4. Gill, W. R., and Vanden Berg, G. E. Soil Dynamics in Tillage and Traction. U.S. Department of Agriculture, Agricultural Handbook 316, 1967.
5. Hansen, R. The Potential for Similitude and Dimensional Analysis in the Design of Flexible Pavements. Cornell Univ., MS thesis, 1966.
6. Kondner, R. L., and Ho, M. M. K. Complex Modulus of a Cohesive Soil From Stress Relaxation Response Using the 1-Sided Fourier Transform. Jour. Applied Physics, Vol. 36, 1965.
7. Krizek, R. J. Phenomenological Soil-Polymer Parallels. Am. Sci., Vol. 56, 1968.
8. Mather, K. B. The Cause of Road Corrugations and the Instability of Surfaces Under Wheel Action. Civil Engineering and Public Works Review, London, Vol. 57, No. 670, 1962.
9. Phelan, R. M. Dynamics of Machinery. McGraw-Hill, New York, 1967.
10. Rickman, R. W. Sonic Radiation for Soil Mechanical Property Measurement. ASAE, Minneapolis, Paper 70-344, 1970.
11. Riley, J. G. The Road Corrugation Phenomenon: A Simulation and Experimental Evaluation. Cornell Univ., PhD thesis, 1971.
12. Terzaghi, K., and Peck, R. B. Soil Mechanics in Engineering Practice. John Wiley and Sons, New York, 1948.
13. Tschebotarioff, G. P., and McAlpin, G. W. Vibratory and Slow Repetitional Loading of Soils. HRB Proc., Vol. 26, 1946, pp. 551-562.
14. Waldron, L. J. Soil Viscoelasticity: Superposition Tests. Proc., Soil Sci. Soc. of Am., 1964.

SPONSORSHIP OF THIS RECORD

GROUP 2—DESIGN AND CONSTRUCTION OF TRANSPORTATION FACILITIES
John L. Beaton, California Division of Highways, chairman

COMPACTION AND STABILIZATION SECTION
Eugene B. McDonald, South Dakota Department of Highways, chairman

Committee on Compaction
John R. Sallberg, Federal Highway Administration, chairman
Robert C. Deen, Leroy D. Graves, Delon Hampton, C. M. Higgins, J. M. Hoover, Eugene Y. Huang, H. W. Humphres, James E. Kelly, Leonard Jay Langfelder, T. F. McMahon, Sidney Mintzer, C. K. Preus, Ernest T. Selig, Charles H. Shepard, T. W. Smith, W. T. Spencer, William G. Weber, Jr.

John W. Guinnee, Highway Research Board staff